Towards the Quantum Internet: Generalised Quantum Network Coding for Large-scale Quantum Communication Networks

Hung Viet Nguyen[1], Zunaira Babar[1], Dimitrios Alanis[1], Panagiotis Botsinis[1], Daryus Chandra[1], Mohd Azri Mohd Izhar[2], Soon Xin Ng[1], and Lajos Hanzo[1]

***Abstract*—Large-scale Quantum Network Coding (LQNC) is conceived for distributing entangled qubits over large-scale quantum communication networks supporting both teleportation and Quantum Key Distribution (QKD). More specifically, the LQNC is characterised by detailing the encoding and decoding process for distributing entangled pairs of qubits to M pairs of source-and-target users connected via a backbone route of N hops. The LQNC-based system advocated is then compared to Entanglement Swapping (ES) based systems for highlighting the benefits of the proposed LQNC.**

I. Introduction and Overview

In the classical domain, network coding [1], [2] is capable of increasing the throughput, while minimising the amount of energy required per packet as well as the delay of packets travelling through the network [3], [4]. This is achieved by allowing the intermediate nodes of the network to combine multiple data packets received via the incoming links before transmission to the destination [5]. Due to its merits, the concept of the network coding has been applied in diverse disciplines [6].

Inspired by its classical counterpart [2], [7], [8], the question arises if the quantum version of network coding exists. Due to the inherent nature of quantum communications, namely that cloning is impossible, negative answers to this cardinal question were suggested in [9], [10]. However, further studies of Quantum Network Coding (QNC) confirm that given the availability of extra resources, such as preshared entanglement [11]–[18] or the abundance of low-cost classical communications [10], [19]–[21], QNC can indeed be made feasible. The important milestones of the QNC history are summarised in Fig. 1.

Entanglement consitutes a valuable enabler of various quantum protocols that are essential for various applications of quantum communications, such as quantum teleportation [22], remote state preparation [23], quantum remote measuring [24] and secret sharing [25]. Entanglement refers to the fact that two or more photons have a very special connection, whereby changing for example the spin of a photon will instantaneously change that of its entangled couterpart. Anecdotally, this phenomenon is referred to as a "spooky action at a distance" by Einstein [26] due to the fact that unlike in electromagnetism, interactions between entangled photons occur instantaneously, regardless of how far apart the photons are. By contrast, electromagnetic interactions are bounded by the speed of light [27].

In such quantum protocols, the entangled qubits have to be distributed to distant nodes. A particularly popular application of the entanglement distribution is Quantum Key Distribution (QKD) [28], which has been gradually finding its way into different practical scenarios, such as satellite communications [29], [30], terrestrial communications [31], [32] and over handheld communication [33], [34]. These advances lay the foundations of the quantum Internet [35]–[37]. Entanglement distribution over a large-scale network consisting of multiple-hops and multiple-nodes can be realised by Entanglement Swapping (ES) [38]–[40] or by QNC [13], [15], [41]. ES may be deemed to be similar to the classic Decode-and-Forward (DF) techniques, which is outperformed by the classical Network Coding (NC) in a number of practical scenarios [42]–[44]. This leads to another intriguing and crucial question, namely whether the QNC is similarly capable of providing a better performance than ES.

As mentioned in Fig. 1, in order to answer the second question, Satoh *et al.* [13] provided quantitative comparisons between the QNC and the ES. Explicitly, it was shown that the fidelity-performance of the ES-based system is superior to that of the QNC-based system in a quantum communication network having $M = 2$ pairs of source-to-target users that are connected via a backbone link having $N = 1$ hop. In this paper, we generalise the QNC of [13], [15] to large-scale quantum communication networks, in order to demonstrate the benefits of our proposed LQNC over ES. Against the above-mentioned background, the novel contribution of our paper is as follows:

- *We formulate the concept of Large-scale Quantum Network Coding (LQNC) that can be used for supporting quantum communication between M pairs of source-to-target users via a backbone link having N hops, where the values of M and N can be chosen arbitrarily.*
- *We devise the general encoding/decoding processes of*

The authors are with the School of Electronics and Computer Science, University of Southampton, Southampton, SO17 1BJ, UK (email: [1] {hvn08r, zb2g10, da4g11, pb1y14, dc2n14, sxn, lh}@ecs.soton.ac.uk) and with Wireless Communication Center and UTM Razak School of Engineering and Advanced Technology, Universiti Teknologi Malaysia, Jalan Sultan Yahya Petra, Kuala Lumpur, 54100, Malaysia (email: [2] mohdazri.kl@utm.my) .

The financial support of the EPSRC under the grant EP/L018659/1, that of the European Research Council, Advanced Fellow Grant and that of the Royal Society's Wolfson Research Merit Award is gratefully acknowledged. Additionally, the authors acknowledge the use of the IRIDIS High Performance Computing Facility, and associated support services at the University of Southampton, in the completion of this work.

LQNC that can be employed in large-scale quantum networks.

- *We provide the quantitative performance analyses of both the individual encoding-and-decoding operations as well as of the system-level encoding-and-decoding processes.*
- *We provide quantitative comparisons to highlight the benefits of the LQNC-based system over ES-based systems, when both the LQNC and ES systems are incorporated into large-scale quantum networks.*
- *We provide design guidelines for the LQNC in beneficial scenarios of large-scale quantum networks.*

The rest of this paper is organised as follows. The relevant background concepts are summarised in Section II for facilitating the presentation of the encoding/decoding operations in Section III. We consider low-complexity scenarios for detailing the encoding/decoding processes and for characterising the error propagation phenomena in Section IV-A and Section V. The fidelity-performance of LQNC is quantitatively analysed in Section VII, in order to confirm the superiority of LQNC over ES in beneficial scenarios. Finally, our LQNC design guidelines are presented in Section VIII along with our conclusions.

II. Preliminary

A. The basis, the Measurement and the Spin-Operator

For the basics of quantum information, refereces [45]–[47] can be used. **For the sake of brevity, we would like to refer the motivated reader to references [45]–[47] for details of the CNOT and Hadamard gates, which are the primary operations used in the encoding/decoding process of our proposed LQNC.** In this section we briefly summarise the details related to the measurement of qubits. In the general case, we may want to measure the state of a qubit represented by $|\varphi\rangle = \alpha|0\rangle + \beta|1\rangle$ in a given I-base denoted by $|I\rangle = I_0|0\rangle + I_1|1\rangle$, where α, β, I_0 and I_1 are complex numbers. The measurement operator M_I associated with the I-base can be formulated as

$$M_I = |I\rangle\langle I|, \tag{1}$$

where we have

$$\begin{aligned} |I\rangle &= I_0|0\rangle + I_1|1\rangle = \begin{bmatrix} I_0 \\ I_1 \end{bmatrix}, \\ \langle I| &= \begin{bmatrix} I_0^* & I_1^* \end{bmatrix}, \end{aligned} \tag{2}$$

with I_0^* and I_1^* being the complex conjugate versions of I_0 and I_1, respectively.

Let us consider examples of the Z-basis and X-basis that are later used in our discussions. The Z-basis consists of a pair of bases, namely $|Z_+\rangle$ and $|Z_-\rangle$, which can be represented by

$$\begin{aligned} |Z_+\rangle &= 1|0\rangle + 0|1\rangle = \begin{bmatrix} 1 \\ 0 \end{bmatrix}, \\ |Z_-\rangle &= 0|0\rangle + 1|1\rangle = \begin{bmatrix} 0 \\ 1 \end{bmatrix}. \end{aligned} \tag{3}$$

Accordingly, the measurement operators in Z-basis are defined by

$$M_{Z_+} = |Z_+\rangle\langle Z_+| = \begin{bmatrix} 1 & 0 \\ 0 & 0 \end{bmatrix}, \tag{4}$$

$$M_{Z_-} = |Z_-\rangle\langle Z_-| = \begin{bmatrix} 0 & 0 \\ 0 & 1 \end{bmatrix}. \tag{5}$$

In the Z-basis, the spin operator δ_Z used for reflecting the rotation in the Z-basis of an electron representing a qubit is defined by

$$\delta_Z = \begin{bmatrix} 1 & 0 \\ 0 & -1 \end{bmatrix}. \tag{6}$$

When applying the spin operator of δ_Z to a qubit of $|\varphi\rangle = \alpha|0\rangle + \beta|1\rangle$, the qubit evolves to

$$|\varphi^{'}\rangle = \delta_Z \begin{bmatrix} \alpha \\ \beta \end{bmatrix} = \begin{bmatrix} \alpha \\ -\beta \end{bmatrix}. \tag{7}$$

Similarly, the X-basis is formed by the pair of bases defined by

$$\begin{aligned} |X_+\rangle &= \frac{1}{\sqrt{2}}|0\rangle + \frac{1}{\sqrt{2}}|1\rangle \equiv \begin{bmatrix} \frac{1}{\sqrt{2}} \\ \frac{1}{\sqrt{2}} \end{bmatrix}, \\ |X_-\rangle &= \frac{1}{\sqrt{2}}|0\rangle - \frac{1}{\sqrt{2}}|1\rangle \equiv \begin{bmatrix} \frac{1}{\sqrt{2}} \\ -\frac{1}{\sqrt{2}} \end{bmatrix}. \end{aligned} \tag{8}$$

Hence, the measurement operators in the X-basis are characterised by

$$M_{X_+} = |X_+\rangle\langle X_+| = \begin{bmatrix} \frac{1}{2} & \frac{1}{2} \\ \frac{1}{2} & \frac{1}{2} \end{bmatrix}, \tag{9}$$

$$M_{X_-} = |X_-\rangle\langle X_-| = \begin{bmatrix} \frac{1}{2} & -\frac{1}{2} \\ -\frac{1}{2} & \frac{1}{2} \end{bmatrix}. \tag{10}$$

Similarly, applying the spin operator δ_X in the X-basis defined by

$$\delta_X = \begin{bmatrix} 0 & 1 \\ 1 & 0 \end{bmatrix} \tag{11}$$

to a qubit of $|\varphi\rangle = \alpha|0\rangle + \beta|1\rangle$ leads to

$$|\varphi^{''}\rangle = \delta_X \begin{bmatrix} \alpha \\ \beta \end{bmatrix} = \begin{bmatrix} \beta \\ \alpha \end{bmatrix}. \tag{12}$$

If we want to measure a qubit of $|\varphi\rangle = \alpha|0\rangle + \beta|1\rangle$, the probability of a specific result obtained by the measurement in the I-basis associated with the measurement operator M_I is calculated by

$$P_{(I)} = \langle\varphi|M_I^\dagger M_I|\varphi\rangle, \tag{13}$$

where $M_I^\dagger$ is the Hermitian conjugate of M_I.

B. Performance metrics

Let us consider a pair of entangled qubits $|AB\rangle$, which can represented by

$$|AB\rangle = \alpha|00\rangle_{AB} + \beta|11\rangle_{AB}, \tag{14}$$

where α and β are complex numbers and we have $|\alpha|^2 + |\beta|^2 = 1$. When a Z-error occurs in the pair, we have

$$|AB\rangle = \alpha|00\rangle_{AB} - \beta|11\rangle_{AB}. \tag{15}$$

Let us consider solely the Z-error, which is caused purely by either qubit $|A\rangle$ or qubit $|B\rangle$, with the probability of $Z_{(A)}$

and $Z_{(B)}$, respectively. **Based on the assumption of the symmetry of the entangled pair of qubits, it is reasonable to assume that we have an equal error probability of $Z_{(A)} = Z_{(B)} = Z_{AB}$ [13]. However, in order to cover the more general case that may have $Z_{(A)} \neq Z_{(B)}$, we use the distinct error probabilities of $Z_{(A)}$ and $Z_{(B)}$ for the pair of qubits $|AB\rangle$.** Hence, the fidelity F of the pair may be calculated by

$$\begin{aligned} F &= 1 - Z_{(A)} - Z_{(B)}, \\ &= 1 - Z_{(A,B)}, \end{aligned} \tag{16}$$

where $Z_{(A,B)} = Z_{(A)} + Z_{(B)}$.

III. Encoding/decoding Operations

Let us commence by detailing the encoding/decoding operations in this section as well as the encoding/decoding processes of LQNC in following sections along with the propagation of a Z-error, which is a likely source of errors imposed by the recently developed quantum materials [48].

A. CONnection operations subjected to Z-error propagation

Let us consider an example of $\text{CON}^{A}_{C->D}$ used for connecting two entangled pairs of qubits, namely $|AB\rangle$ and $|CD\rangle$. The operation $\text{CON}^{A}_{C->D}$ is performed by the circuit portrayed in Fig. 2(a), which carries out the steps listed in Fig. 2(b).

According to Fig. 2(a) and Fig. 2(b), an initial state is assumed to be as follows

$$|\Psi\rangle_{init} = \frac{1}{2}\left(|00\rangle_{AB} + |11\rangle_{AB}\right)\left(|00\rangle_{CD} + |11\rangle_{CD}\right) \tag{17}$$

As mentioned in Section II-B, we assume to have a Z error at either of the two qubits in a pair. Then, after Step 1 of Fig. 2(b) carrying out $\text{CNOT}^{A->C}$, the initial state is changed to

$$\begin{aligned} |\Psi\rangle_{C1} &= \frac{1}{2}|00\rangle_{AB}\left(|00\rangle_{CD}\underbrace{+|11\rangle_{CD}}_{Z_{(C,D)}}\right) + \\ &\quad \frac{1}{2}\underbrace{|11\rangle_{AB}}_{Z_{(A,B)}}\left(|10\rangle_{CD}\underbrace{+|01\rangle_{CD}}_{Z_{(C,D)}}\right), \end{aligned} \tag{18}$$

where $Z_{(A,B)}$ and $Z_{(C,D)}$ are Z-errors contributed by qubit $|A\rangle, |B\rangle, |C\rangle$ and $|D\rangle$, respectively. **Explicitly, the notation $\underbrace{|01\rangle_{CD}}_{Z_{(C,D)}}$ represents the current state of qubits $|CD\rangle = |01\rangle$, which may contain a Z-error of qubit $|C\rangle$ and of qubit $|D\rangle$.**

Then, as seen in Fig. 2(a), the Z-measurement of $|C\rangle$ is carried out by M^Z, and the measurement result m_r is transmitted via an error-free classical channel to the location of qubit $|D\rangle$, where the result m_r is used for controlling the δ_X operator acting on $|D\rangle$. As a result of the measurement in Section II-A, a $Z_{(C)}$ error is inflicted upon the resultant state, when having $m_r = 0$, yielding

$$|\Psi\rangle_{C2} = \frac{1}{\sqrt{2}}|000\rangle_{ABD} \underbrace{+\frac{1}{\sqrt{2}}|111\rangle_{ABD}}_{Z_{(A,B,C,D)}}. \tag{19}$$

By contrast, in the case of having $m_r = 1$, the state becomes

$$|\Psi\rangle_{C3} = \frac{1}{\sqrt{2}}|00\underbrace{1}_{Z_{(C,D)}}\rangle_{ABD} + \frac{1}{\sqrt{2}}|\underbrace{11}_{Z_{(A,B)}}0\rangle_{ABD}. \tag{20}$$

Since we have $m_r = 1$, δ_X is applied to $|D\rangle$ to convert $|\Psi\rangle_{C3}$ of Eq. (20) to

$$|\Psi\rangle_{C4} = \frac{1}{\sqrt{2}}|000\rangle_{ABD} \underbrace{+\frac{1}{\sqrt{2}}|111\rangle_{ABD}}_{Z_{(A,B,C,D)}}. \tag{21}$$

Hence, regardless of the result of the Z-measurement m_r, the resultant state $|\Psi\rangle_{Cr}$ after the CON operation becomes:

$$|\Psi\rangle_{Cr} = \frac{1}{\sqrt{2}}|000\rangle_{ABD} \underbrace{+\frac{1}{\sqrt{2}}|111\rangle_{ABD}}_{Z_{(A,B,C,D)}}. \tag{22}$$

If we assume the initial fidelity of each Bell pair to be $F_{AB} = F_{CD} = F$, it can be readily seen from Eq. (22) that Z-error occurs at $|\Psi\rangle_{Cr}$, when a Z-error happens either at $|AB\rangle$ or at $|CD\rangle$, which happens with the probability of $2F(1-F)$. Accordingly, the fidelity F_{CON} of the system after the CON operation can be calculated by

$$F_{CON} = 1 - 2F(1-F). \tag{23}$$

The CON operation can be generalised to the case, when the initial state is in the following form [15]

$$|\Psi\rangle_{init} = \left(\alpha|\Psi_0\rangle|0\rangle_A + \beta|\Psi_1\rangle|1\rangle_A\right)|\Psi^+\rangle_{CD}|\Phi\rangle, \tag{24}$$

where $|\alpha|^2 + |\beta|^2 = 1$ and $|\Psi_0\rangle$, $|\Psi_1\rangle$ and $|\Phi\rangle$ are arbitrary quantum states. After applying the CON operation to $|\Psi\rangle_{init}$ of Eq. (24), the following final state is obtained

$$|\Psi\rangle_{Cf} = \left(\alpha|\Psi_0\rangle|00\rangle_{AD} + \beta|\Psi_1\rangle|11\rangle_{AD}\right)|\Phi\rangle. \tag{25}$$

B. ADD operation with Z-error propagation

Let us now consider an example of the $\text{ADD}^{D,H}_{I->J}$ operation, which uses multiple control qubits, namely $|D\rangle$ and $|H\rangle$, in order to compress the quantum information of the control qubits into the target qubit $|I\rangle$. Then the compressed information is transmitted over a quantum transmission link by performing a measurement-and-control procedure, namely the measurement in the Z-basis and the spin operator δ_X. The circuit of the operation $\text{ADD}^{D,H}_{I->J}$ is portrayed in Fig. 3(a), which includes 3 steps, as detailed in Fig. 3(b).

Let us consider the example of an initial state as

$$\begin{aligned} |\Psi\rangle_{Ai} &= \frac{1}{2\sqrt{2}}\left(|00\rangle_{CD} + \underbrace{|11\rangle_{CD}}_{Z_{(C,D)}}\right)\left(|00\rangle_{GH} + \underbrace{|11\rangle_{GH}}_{Z_{(G,H)}}\right) \\ &\quad \left(|00\rangle_{IJ} + \underbrace{|11\rangle_{IJ}}_{Z_{(I,J)}}\right). \end{aligned} \tag{26}$$

Step 1 of Fig. 3(b) is to perform $\text{CNOT}_{D->I}$ that converts the state $|\Psi\rangle_{Ai}$ of Eq. (26) to

$$|\Psi\rangle_{A1} = \frac{1}{2\sqrt{2}}|00\rangle_{CD}\left(|00\rangle_{IJ} + \underbrace{|11\rangle_{IJ}}_{Z_{(I,J)}}\right)\left(|00\rangle_{GH} + \underbrace{|11\rangle_{GH}}_{Z_{(G,H)}}\right)|\Psi\rangle_{A5}$$
$$+\frac{1}{2\sqrt{2}}\underbrace{|11\rangle_{CD}}_{Z_{(C,D)}}\left(|10\rangle_{IJ} + \underbrace{|01\rangle_{IJ}}_{Z_{(I,J)}}\right)\left(|00\rangle_{GH} + \underbrace{|11\rangle_{GH}}_{Z_{(G,H)}}\right). \quad (27)$$

Similarly, Step 2 of Fig. 3(b) performs $\text{CNOT}_{H->I}$ that changes the state $|\Psi\rangle_{A1}$ of Eq. (27) to

$$|\Psi\rangle_{A2} = \frac{1}{2\sqrt{2}}|00\rangle_{CD}|00\rangle_{GH}\left(|00\rangle_{IJ} + \underbrace{|11\rangle_{IJ}}_{Z_{(I,J)}}\right) +$$
$$\frac{1}{2\sqrt{2}}\underbrace{|11\rangle_{CD}}_{Z_{(C,D)}}|00\rangle_{GH}\left(|10\rangle_{IJ} + \underbrace{|01\rangle_{IJ}}_{Z_{(I,J)}}\right) +$$
$$\frac{1}{2\sqrt{2}}|00\rangle_{CD}\underbrace{|11\rangle_{GH}}_{Z_{(G,H)}}\left(|10\rangle_{IJ} + \underbrace{|01\rangle_{IJ}}_{Z_{(I,J)}}\right) +$$
$$\frac{1}{2\sqrt{2}}\underbrace{|11\rangle_{CD}}_{Z_{(C,D)}}\underbrace{|11\rangle_{GH}}_{Z_{(G,H)}}\left(|00\rangle_{IJ} + \underbrace{|11\rangle_{IJ}}_{Z_{(I,J)}}\right). \quad (28)$$

Then, in Step 3 of Fig. 3(b), the qubit $|I\rangle$ is measured in the Z basis in order to use the measurement result m_r to control the spin operation δ_X acting on qubit $|J\rangle$. Accordingly, when we have the measurement result of $m_r = 0$, the state $|\Psi\rangle_{A2}$ of Eq. (28) becomes

$$|\Psi\rangle_{A3} = \frac{1}{2}\left(|00\rangle_{CD}|00\rangle_{GH}|0\rangle_J + \underbrace{|11\rangle_{CD}}_{Z_{(C,D)}}|00\rangle_{GH}\underbrace{|1\rangle_J}_{Z_{(I,J)}}\right)$$
$$+\frac{1}{2}\left(|00\rangle_{CD}\underbrace{|11\rangle_{GH}}_{Z_{(G,H)}}\underbrace{|1\rangle_J}_{Z_{(I,J)}} + \underbrace{|11\rangle_{CD}}_{Z_{(C,D)}}\underbrace{|11\rangle_{GH}}_{Z_{(G,H)}}|0\rangle_J\right)$$
$$= \frac{1}{2}\left(|00\rangle_{CD}|00\rangle_{GH} + \underbrace{|11\rangle_{CD}}_{Z_{(C,D)}}\underbrace{|11\rangle_{GH}}_{Z_{(G,H)}}\right)|0\rangle_J$$
$$+\frac{1}{2}\left(\underbrace{|11\rangle_{CD}}_{Z_{(C,D)}}|00\rangle_{GH} + |00\rangle_{CD}\underbrace{|11\rangle_{GH}}_{Z_{(G,H)}}\right)\underbrace{|1\rangle_J}_{Z_{(I,J)}} \quad (29)$$

By contrast, if $m_r = 1$ is obtained, state $|\Psi\rangle_{A2}$ of Eq. (28) evolves to

$$|\Psi\rangle_{A4} = \frac{1}{2}\left(|00\rangle_{CD}|00\rangle_{GH}\underbrace{|1\rangle_J}_{Z_{(I,J)}} + \underbrace{|11\rangle_{CD}}_{Z_{(C,D)}}|00\rangle_{GH}|0\rangle_J\right) \quad (30)$$
$$+\frac{1}{2}\left(|00\rangle_{CD}\underbrace{|11\rangle_{GH}}_{Z_{(G,H)}}|0\rangle_J + \underbrace{|11\rangle_{CD}}_{Z_{(C,D)}}\underbrace{|11\rangle_{GH}}_{Z_{(G,H)}}\underbrace{|1\rangle_J}_{Z_{(I,J)}}\right)$$

Then, the spin operation δ_X is applied to $|J\rangle$ in Eq. (30) to obtain the state

$$|\Psi\rangle_{A5} = \frac{1}{2}\left(|00\rangle_{CD}|00\rangle_{GH}|0\rangle_J + \underbrace{|11\rangle_{CD}}_{Z_{(C,D)}}|00\rangle_{GH}\underbrace{|1\rangle_J}_{Z_{(I,J)}}\right)$$
$$+\frac{1}{2}\left(|00\rangle_{CD}\underbrace{|11\rangle_{GH}}_{Z_{(G,H)}}\underbrace{|1\rangle_J}_{Z_{(I,J)}} + \underbrace{|11\rangle_{CD}}_{Z_{(C,D)}}\underbrace{|11\rangle_{GH}}_{Z_{(G,H)}}|0\rangle_J\right)$$
$$= |\Psi\rangle_{A3}\,. \quad (31)$$

It can be readily inferred from Eq. (29) and Eq. (31) that after the ADD operation, the system will have no Z error when $Z_{(I,J)} + Z_{(G,H)} \neq 1$ and $Z_{(I,J)} + Z_{(C,D)} \neq 1$ and $Z_{(I,J)} + Z_{(C,D)} \neq 1$ is satisfied, which occurs with a probability of

$$F_{\text{ADD}} = F^3 + (1-F)^3, \quad (32)$$

where we assume that all three pairs have the same fidelity $F_{IJ} = F_{CD} = F_{GH}$.

Let us now generalise the ADD operation applying it to an initial state as [15]

$$|\Psi\rangle_{Ai} = (\alpha|\Psi_0\rangle|0\rangle_D + \beta|\Psi_1\rangle|1\rangle_D)$$
$$(\gamma|\Phi_0\rangle|0\rangle_H + \delta|\Phi_1\rangle|1\rangle_H)\,|\Psi^+\rangle_{IJ}|\Phi\rangle, \quad (33)$$

where $|\alpha|^2 + |\beta|^2 = |\gamma|^2 + |\delta|^2 = 1$ and $|\Psi_0\rangle$, $|\Psi_1\rangle$, $|\Phi_0\rangle$, $|\Phi_1\rangle$ and $|\Phi\rangle$ are arbitrary quantum states. After applying the $\text{ADD}^{D,H}_{I->J}$ operation to $|\Psi\rangle_{Ai}$ of Eq. (33), the following final result is obtained [15]

$$|\Psi\rangle_{Af} = (\alpha\gamma|\Psi_0\rangle|\Phi_0\rangle|00\rangle_{DH} + \beta\delta|\Psi_1\rangle|\Phi_1\rangle|11\rangle_{DH})\,|0\rangle_J|\Phi\rangle$$
$$+\,(\alpha\delta|\Psi_0\rangle|\Phi_1\rangle|01\rangle_{DH} + \beta\gamma|\Psi_1\rangle|\Phi_0\rangle|11\rangle_{DH})\,|1\rangle_J|\Phi\rangle. \quad (34)$$

C. FANout operation with Z-error propagation

Let us now consider an example of the $\text{FAN}^J_{K->L,M->N}$ operation, which is invoked for connecting a qubit $|J\rangle$ to two pairs of entangled qubits, namely to $|KL\rangle$ and $|MN\rangle$. The implementation of the $\text{FAN}^J_{K->L,M->N}$ operation is illustrated in Fig. 4(a), which can be summarised by the steps in Fig. 4(b).

As seen in Fig. 4(a), let us assume the initial state before applying the FAN operation to be

$$|\Psi\rangle_{Fi} = \frac{1}{2\sqrt{2}}\left(|0\rangle_J + \underbrace{|1\rangle_J}_{Z_J}\right)\left(|00\rangle_{KL} + \underbrace{|11\rangle_{KL}}_{Z_{(K,L)}}\right)$$
$$\left(|00\rangle_{MN} + \underbrace{|11\rangle_{MN}}_{Z_{(M,N)}}\right). \quad (35)$$

After Step 1 and Step 2 of Fig. 4(b), where $\text{CNOT}_{J->K}$ and $\text{CNOT}_{J->M}$ are carried out, the state $|\Psi\rangle_{Fi}$ of Eq. (35)

becomes

$$|\Psi\rangle_{F1} = \frac{1}{2\sqrt{2}}|0\rangle_J \left(|00\rangle_{KL} + \underbrace{|11\rangle_{KL}}_{Z_{(K,L)}}\right)\left(|00\rangle_{MN} + \underbrace{|11\rangle_{MN}}_{Z_{(M,N)}}\right) + \frac{1}{2\sqrt{2}}\underbrace{|1\rangle_J}_{Z_J}\left(|10\rangle_{KL} + \underbrace{|01\rangle_{KL}}_{Z_{(K,L)}}\right)\left(|10\rangle_{MN} + \underbrace{|01\rangle_{MN}}_{Z_{(M,N)}}\right). \quad (36)$$

At Step 3 in Fig. 4(b), qubit $|K\rangle$ is measured in the Z basis, and then the measurement result is used for controlling the spin operation δ_X acting on qubit $|L\rangle$. If the measurement result $m_r = 0$ is obtained, the state $|\Psi\rangle_{F1}$ of Eq. (36) becomes

$$|\Psi\rangle_{F3} = \frac{1}{2}|00\rangle_{JL}\left(|00\rangle_{MN} + \underbrace{|11\rangle_{MN}}_{Z_{(M,N)}}\right) + \frac{1}{2}\underbrace{|11\rangle_{JL}}_{Z_J, Z_{(K,L)}}\left(|10\rangle_{MN} + \underbrace{|01\rangle_{MN}}_{Z_{(M,N)}}\right). \quad (37)$$

By contrast, if the measurement result $m_r = 1$ is obtained, the state $|\Psi\rangle_{F1}$ of Eq. (36) evolves to

$$|\Psi\rangle_{F4} = \frac{1}{2}\underbrace{|01\rangle_{JL}}_{Z_{(K,L)}}\left(|00\rangle_{MN} + \underbrace{|11\rangle_{MN}}_{Z_{(M,N)}}\right) + \frac{1}{2}\underbrace{|10\rangle_{JL}}_{Z_J}\left(|10\rangle_{MN} + \underbrace{|01\rangle_{MN}}_{Z_M}\right). \quad (38)$$

Accordingly, the spin operation δ_X is applied to $|L\rangle$ of Eq. (38) for arriving to the state

$$|\Psi\rangle_{F5} = \frac{1}{2}|00\rangle_{JL}\left(|00\rangle_{MN} + \underbrace{|11\rangle_{MN}}_{Z_{(M,N)}}\right) + \frac{1}{2}\underbrace{|11\rangle_{JL}}_{Z_J, Z_{(K,L)}}\left(|10\rangle_{MN} + \underbrace{|01\rangle_{MN}}_{Z_{(M,N)}}\right). \quad (39)$$

After this step, we can readily see that $|\Psi\rangle_{F5}$ of Eq. (39) becomes identical to $|\Psi\rangle_{F3}$ of Eq. (37).

Similarly, at Step 4 of Fig. 4(b), the qubit $|M\rangle$ is measured in the Z basis in order to use the measurement result to control δ_X that operates on qubit $|N\rangle$. Regardless of the measurement result of $|M\rangle$, the following state is obtained

$$|\Psi\rangle_{F6} = \frac{1}{\sqrt{2}}\left(|000\rangle_{JLN} + \underbrace{|111\rangle_{JLN}}_{Z_{(J,K,L,M,N)}}\right). \quad (40)$$

As a result, the fidelity of the system after the FANOUT operator can be quantified by

$$F_{\text{FAN}} = 1 - (1-F)^3 - 3(1-F)F^2, \quad (41)$$

where we assume that the fidelity value of the single qubit ($|J\rangle$) and of the pairs ($|KL\rangle$ and $|MN\rangle$) of qubits are equal, $F = F_J = F_{KL} = F_{MN}$.

It can be generalised from Eq. (35) and Eq. (40) that given an initial state of

$$|\Psi\rangle_{Fi} = (\alpha|0\rangle_J + \beta|1\rangle_J)\,|\Psi^+\rangle_{KL}|\Psi^+\rangle_{MN}, \quad (42)$$

applying the $\text{FAN}^J_{K->L,M->N}$ operation to the initial state leads to the following final state

$$|\Psi\rangle_{Ff} = \alpha|000\rangle_{JLN} + \beta|111\rangle_{JLN}. \quad (43)$$

D. REMoval operation subjected to Z errors

The REM operation is conceived for deleting a resource qubit of a quantum state by applying a Hadamard gate and then a Z-measurement of the resource qubit. Then, the measurement result is used for controlling the δ_Z operation acting on the associated target qubit. The REM operation is carried out by the circuit illustrated in Fig. 5(a), which is summarised in Fig. 5(b).

Let us consider an example of applying the $\text{REM}_{D->A}$ operation to an initial state as

$$|\Psi\rangle_{Ri} = \frac{1}{\sqrt{2}}\left(|000\rangle_{ABD} + \underbrace{|111\rangle_{ABD}}_{Z_{(A,B,D)}}\right). \quad (44)$$

Firstly, according to Fig. 5(b), the Hadamard gate is applied to qubit $|D\rangle$. As mentioned in Section II-A, the Hadamard basis is denoted as

$$|+\rangle = H(|0\rangle) = \frac{1}{\sqrt{2}}(|0\rangle + |1\rangle),$$
$$|-\rangle = H(|1\rangle) = \frac{1}{\sqrt{2}}(|0\rangle - |1\rangle). \quad (45)$$

Then the state $|\Psi\rangle_{Ri}$ of Eq. (44) is changed to

$$|\Psi\rangle_{R1} = \frac{1}{\sqrt{2}}\left(|00+\rangle_{ABD} + \underbrace{|11-\rangle_{ABD}}_{Z_{(A,B,D)}}\right). \quad (46)$$

Secondly, as detailed in Fig. 5(b) and illustrated in Fig. 5(a), qubit $|D\rangle$ is measured in the Z basis. If we have the measurement result $m_r = 0$, the state becomes

$$|\Psi\rangle_{R2} = \frac{1}{\sqrt{2}}\left(|00\rangle_{AB} + \underbrace{|11\rangle_{AB}}_{Z_{(A,B,D)}}\right). \quad (47)$$

By contrast, if we have the measurement result $m_r = 1$, the state becomes

$$|\Psi\rangle_{R3} = \frac{1}{\sqrt{2}}\left(|00\rangle_{AB} - \underbrace{|11\rangle_{AB}}_{Z_{(A,B,D)}}\right). \quad (48)$$

Given the measurement result $m_r = 1$, the operation δ_Z is applied to the target qubit $|A\rangle$ to convert the state $|\Psi\rangle_{R3}$ of

Eq. (48) to

$$|\Psi\rangle_{R4} = \frac{1}{\sqrt{2}}\left(|00\rangle_{AB} + \underbrace{|11\rangle_{AB}}_{Z_{(A,B,D)}}\right), \quad (49)$$

where the δ_Z operation is detailed in Section II-A. Having $|\Psi\rangle_{R2} \equiv |\Psi\rangle_{R4}$ as the resultant state, we may generalise the result of the REM operation applied to an initial state as

$$|\Psi\rangle_{Ri} = (\alpha|00\rangle_{AD}|\Psi_0\rangle + \beta|11\rangle_{AD}|\Psi_1\rangle)\,|\Phi\rangle, \quad (50)$$

where $|\alpha|^2+|\beta|^2 = 1$, $|\Psi_0\rangle$, $|\Psi_1\rangle$ and $|\Phi\rangle$ are arbitrary quantum states. After applying the operation $\text{REM}_{D->A}$ to the state $|\Psi\rangle_{Ri}$ of Eq. (50), we obtain the following final state [15]

$$|\Psi\rangle_{Rf} = (\alpha|0\rangle_A|\Psi_0\rangle + \beta|1\rangle_A|\Psi_1\rangle)\,|\Phi\rangle. \quad (51)$$

E. Remove-and-add operation subject to Z errors

The Remove-and-add (REMADD) operation may be used for deleting the target qubit employed in the ADD operation. The REMADD operation is carried out by the circuit detailed in Fig. 6(a), which may be summarised in the following steps detailed in Fig. 6(b).

Let us consider the example of applying the $\text{REMADD}_{A->B,C}$ operation illustrated in Fig. 6 to an initial state as

$$|\Psi\rangle_{RAi} = \frac{1}{\sqrt{4}}\left(|00\rangle_{BC} + \underbrace{|11\rangle_{BC}}_{Z_B,Z_C}\right)|0\rangle_A + \frac{1}{\sqrt{4}}\left(\underbrace{|01\rangle_{BC}}_{Z_C} + \underbrace{|10\rangle_{BC}}_{Z_B}\right)\underbrace{|1\rangle_A}_{Z_A}. \quad (52)$$

Accordingly, at Step 1 of Fig. 6(b), where the Hadamard gate is applied to qubit $|A\rangle$, the state of $|\Psi\rangle_{RAi}$ becomes

$$|\Psi\rangle_{RA1} = \frac{1}{\sqrt{4}}\left(|00\rangle_{BC} + \underbrace{|11\rangle_{BC}}_{Z_B,Z_C}\right)\frac{1}{\sqrt{2}}(|0\rangle_A + |1\rangle_A) + \frac{1}{\sqrt{4}}\left(\underbrace{|01\rangle_{BC}}_{Z_C} + \underbrace{|10\rangle_{BC}}_{Z_B}\right)\underbrace{\frac{1}{\sqrt{2}}(|0\rangle_A - |1\rangle_A)}_{Z_A}. \quad (53)$$

Then, at Step 2 of Fig. 6(b) $|A\rangle$ is measured. If we have the measurement result of $m_r = 0$, the state is changed to

$$|\Psi\rangle_{RA2} = \frac{1}{\sqrt{4}}\left(|00\rangle_{BC} + \underbrace{|11\rangle_{BC}}_{Z_B,Z_C}\right) + \frac{1}{\sqrt{4}}\left(\underbrace{|01\rangle_{BC}}_{Z_C,Z_A} + \underbrace{|10\rangle_{BC}}_{Z_B,Z_A}\right) = \frac{1}{\sqrt{4}}\left(|0\rangle_B + \underbrace{|1\rangle_B}_{Z_B,Z_A}\right)\left(|0\rangle_C + \underbrace{|1\rangle_C}_{Z_C,Z_A}\right). \quad (54)$$

By contrast, if we have the measurement result of $m_r = 1$, the state $|\Psi\rangle_{RA1}$ of Eq. (53) becomes

$$|\Psi\rangle_{RA3} = \frac{1}{\sqrt{4}}\left(|00\rangle_{BC} + \underbrace{|11\rangle_{BC}}_{Z_B,Z_C}\right) - \frac{1}{\sqrt{4}}\left(\underbrace{|01\rangle_{BC}}_{Z_C,Z_A} + \underbrace{|10\rangle_{BC}}_{Z_B,Z_A}\right) = \frac{1}{\sqrt{4}}\left(|0\rangle_B - \underbrace{|1\rangle_B}_{Z_B,Z_A}\right)\left(|0\rangle_C - \underbrace{|1\rangle_C}_{Z_C,Z_A}\right). \quad (55)$$

As a result of having the measurement result $m_r = 1$, the operation δ_Z is applied to the target qubit $|B\rangle$ and $|C\rangle$ to bring the state $|\Psi\rangle_{RA3}$ of Eq. (55) to

$$|\Psi\rangle_{RA4} = \frac{1}{\sqrt{4}}\left(|0\rangle_B + \underbrace{|1\rangle_B}_{Z_B,Z_A}\right)\left(|0\rangle_C + \underbrace{|1\rangle_C}_{Z_C,Z_A}\right) \quad (56)$$

Hence, $|\Psi\rangle_{RA2} \equiv |\Psi\rangle_{RA4}$ is the resultant state.

It can be generalised from state $|\Psi\rangle_{RAi}$ of Eq. (52) and state $|\Psi\rangle_{RA4}$ of Eq. (56) that if the following initial state is given

$$|\Psi\rangle_{RAi} = (\alpha\gamma|00\rangle_{CB} + \beta\delta|11\rangle_{CB})\,|0\rangle_A + (\alpha\delta|01\rangle_{CB} + \beta\gamma|10\rangle_{CB})\,|1\rangle_A, \quad (57)$$

applying $\text{REMADD}_{A->B,C}$ to the state $|\Psi\rangle_{RAi}$ will lead to the final state of [15]

$$|\Psi\rangle_{RAf} = (\alpha|0\rangle_B + \beta|1\rangle_B)\,(\gamma|0\rangle_C + \delta|1\rangle_C). \quad (58)$$

IV. N-HOP NETWORK SUPPORTING $M = 2$ PAIRS OF USERS

In the following sections, we first detail the encoding/decoding processes in the system detailed in Section IV-A. The system is capable of distributing entanglement to $M = 2$ pairs of users via an $N = 1$ hop backbone link, as portrayed in Fig. 7(a). Then, we further formulate the system illustrated in Fig. 7(b) of Section IV-B, which consists of an N-hop backbone and supports $M = 2$ pairs of users, where the number of hops N may be arbitrarily chosen. Ultimately, we generalised the system in Section IV-A and Section IV-B, in order to introduce in Section V the large-scale system associated with arbitrarily large number of M-pairs and N-hops in Fig. 7(c). The system is termed as the Large-scale Quantum Network Coding (LQNC) system.

A. Encoding/decoding processes for systems having $N = 1$ hop supporting $M = 2$ pairs

Let us first detail the QNC system of Fig. 7(a) introduced in [13], [15], where $M = 2$ pairs of entangled qubits are distributed in a network connected via an $N = 1$ hop backbone link. Accordingly, the encoding/decoding processes used for the scheme are summarised in the seven phases detailed in Table I.

Initially, the system presented in Fig. 7(a) has seven entangled pairs of qubits, hence we have the corresponding initial system state of

$$|\Psi\rangle_{init} = |MN\rangle|KL\rangle|IJ\rangle|GH\rangle|EF\rangle|CD\rangle|AB\rangle. \quad (59)$$

Phases	$\text{QNC}_{(N=1,M=2)}$ Operations
1	$\text{CON}^{A}_{C->D}$ at S_1 and R_1, $\text{CON}^{E}_{G->H}$ at S_2 and R_1
2	$\text{ADD}^{D,H}_{I->J}$ at R_1 and R_2
3	$\text{FAN}^{J}_{K->L,M->N}$ at R_2, T_1 and T_2
4	$\text{CNOT}^{L,B}$ at T_1, $\text{CNOT}^{N,F}$ at T_2
5	$\text{REM}_{L->J}$ at R_2 and T_1, $\text{REM}_{N->J}$ at R_2 and T_2
6	$\text{REMADD}_{J->D,H}$ at R_1 and R_2
7	$\text{REM}_{D->A}$ at R_1 and S_1, $\text{REM}_{H->E}$ at R_1 and S_2

TABLE I: Encoding/decoding process of QNC distributing $M = 2$ entangled pairs of qubits via the $N = 1$-hop backbone network portrayed in Fig. 7(a).

1) Phase 1 of $QNC_{(N=1,M=2)}$: is to carry out the operations in Table I, namely $\text{CON}^{A}_{C->D}$ and $\text{CON}^{E}_{G->H}$, which converts $|\Psi\rangle_{init}$ of Eq. (59) to

$$|\Psi\rangle_{P1} = |MN\rangle|KL\rangle|IJ\rangle \underbrace{\frac{1}{\sqrt{2}}\left(|000\rangle_{EFH} \underbrace{+|111\rangle_{EFH}}_{Z_{(E,F,G,H)}}\right)}_{\text{From CON}^{E}_{G->H}} \underbrace{\frac{1}{\sqrt{2}}\left(|000\rangle_{ABD} \underbrace{+|111\rangle_{ABD}}_{Z_{(A,B,C,D)}}\right)}_{\text{From CON}^{A}_{C->D}}, \quad (60)$$

where the details of $\text{CON}^{A}_{C->D}$ and $\text{CON}^{E}_{G->H}$ are presented in Section III-A.

2) Phase 2 of $QNC_{(N=1,M=2)}$: is to perform $\text{ADD}^{D,H}_{I->J}$ of Table I, in order to lead to the resultant state as

$$\begin{aligned}|\Psi\rangle_{P2} &= |MN\rangle|KL\rangle|000\rangle_{EFH}|000\rangle_{ABD}|0\rangle_J + \\ &\quad |MN\rangle|KL\rangle \underbrace{|111\rangle_{ABD}|111\rangle_{EFH}}_{Z_{(E,F,G,H,A,B,C,D)}}|0\rangle_J + \\ &\quad |MN\rangle|KL\rangle \underbrace{|000\rangle_{EFH}|111\rangle_{ABD}}_{Z_{(A,B,C,D)}} \underbrace{|1\rangle_J}_{\underbrace{Z_{(I,J)}}_{\text{From ADD}^{D,H}_{I->J}}} + \\ &\quad |MN\rangle|KL\rangle \underbrace{|111\rangle_{EFH}|000\rangle_{ABD}}_{Z_{(E,F,G,H)}} \underbrace{|1\rangle_J}_{\underbrace{Z_{(I,J)}}_{\text{From ADD}^{D,H}_{I->J}}}, \end{aligned} \quad (61)$$

where the details of the $\text{ADD}^{D,H}_{I->J}$ operation are provided in Section III-B.

3) Phase 3 of $QNC_{(N=1,M=2)}$: $\text{FAN}^{J}_{K->L,M->N}$ in Table I is executed at R_2, T_1 and T_2 for connecting qubit $|J\rangle$ to the entangled pairs of qubits, namely to $|KL\rangle$ and $|MN\rangle$, converting $|\Psi\rangle_{P2}$ of Eq. (61) to the following state:

$$\begin{aligned}|\Psi\rangle_{P3} &= |000\rangle_{EFH}|000\rangle_{ABD}|000\rangle_{JNL} + \\ &\quad \underbrace{|111\rangle_{ABD}|111\rangle_{EFH}}_{Z_{(E,F,G,H,A,B,C,D)}}|000\rangle_{JNL} + \\ &\quad \underbrace{|000\rangle_{EFH}|111\rangle_{ABD}}_{Z_{(A,B,C,D)}} \underbrace{|111\rangle_{JLN}}_{\underbrace{Z_{(I,J,K,L,M,N)}}_{\text{From FAN}^{J}_{K->L,M->N}}} + \\ &\quad \underbrace{|111\rangle_{EFH}|000\rangle_{ABD}}_{Z_{(E,F,G,H)}} \underbrace{|111\rangle_{JLN}}_{\underbrace{Z_{(I,J,K,L,M,N)}}_{\text{From FAN}^{J}_{K->L,M->N}}}, \end{aligned} \quad (62)$$

where the operator $\text{FAN}^{J}_{K->L,M->N}$ detailed in Section III-C is applied.

4) Phase 4 of $QNC_{(N=1,M=2)}$: is to perform $\text{CNOT}_{L->B}$ at T_1 and $\text{CNOT}_{N->F}$ at T_2 of Table I, in order for the system state of Eq. (62) to evolve to

$$\begin{aligned}|\Psi\rangle_{P4} &= |000\rangle_{EFH}|000\rangle_{ABD}|000\rangle_{JNL} + \\ &\quad \underbrace{|111\rangle_{ABD}|111\rangle_{EFH}}_{Z_{(E,F,G,H,A,B,C,D)}}|000\rangle_{JNL} + \\ &\quad \underbrace{|010\rangle_{EFH}|101\rangle_{ABD}}_{Z_{(A,B,C,D)}} \underbrace{|111\rangle_{JLN}}_{Z_{(I,J,K,L,M,N)}} + \\ &\quad \underbrace{|101\rangle_{EFH}|010\rangle_{ABD}}_{Z_{(E,F,G,H)}} \underbrace{|111\rangle_{JLN}}_{Z_{(I,J,K,L,M,N)}}. \end{aligned} \quad (63)$$

5) Phase 5 of $QNC_{(N=1,M=2)}$: to perform $\text{REM}_{L->J}$ at R_2 and T_1 as well as $\text{REM}_{N->J}$ at R_2 and T_2 of Table I for arriving at the state of

$$\begin{aligned}|\Psi\rangle_{P5} &= |000\rangle_{EFH}|000\rangle_{ABD}|0\rangle_J + \\ &\quad \underbrace{|111\rangle_{ABD}|111\rangle_{EFH}}_{Z_{(E,F,G,H,A,B,C,D)}}|0\rangle_J + \\ &\quad \underbrace{|010\rangle_{EFH}|101\rangle_{ABD}}_{Z_{(A,B,C,D)}} \underbrace{|1\rangle_J}_{Z_{(I,J,K,L,M,N)}} + \\ &\quad \underbrace{|101\rangle_{EFH}|010\rangle_{ABD}}_{Z_{(E,F,G,H)}} \underbrace{|1\rangle_J}_{Z_{(I,J,K,L,M,N)}}, \end{aligned} \quad (64)$$

when applying the general results of the REM operation detailed in Section III-D.

6) Phase 6 of $QNC_{(N=1,M=2)}$: to accomplish the operation $\text{REMADD}_{J->D,H}$ of Table I to remove qubit $|J\rangle$ at R_1 and R_2 for getting to the state of

$$\begin{aligned}|\Psi\rangle_{P6} &= |000\rangle_{EFH}|000\rangle_{ABD} + \\ &\quad \underbrace{|111\rangle_{ABD}|111\rangle_{EFH}}_{Z_{(E,F,G,H,A,B,C,D)}} + \\ &\quad \underbrace{|010\rangle_{EFH}|101\rangle_{ABD}}_{Z_{(A,B,C,D,I,J,K,L,M,N)}} + \\ &\quad \underbrace{|101\rangle_{EFH}|010\rangle_{ABD}}_{Z_{(E,F,G,H,I,J,K,L,M,N)}}, \end{aligned} \quad (65)$$

where we apply the manipulations of $\text{REMADD}_{J->D,H}$ detailed in Section III-E.

7) Phase 7 of QNC$_{(N=1,M=2)}$: is for carrying out REM$_{D->A}$ of Table I at R_1 and S_1 as well as REM$_{H->E}$ of Table I at R_1 and S_2. As a result, state $|\Psi\rangle_{P6}$ of Eq. (65) is changed to the final state of

$$|\Psi\rangle_{P7} = |00\rangle_{EF}|00\rangle_{AB} + \underbrace{|11\rangle_{AB}|11\rangle_{EF}}_{Z_{(E,F,G,H,A,B,C,D)}} + \underbrace{|01\rangle_{EF}|10\rangle_{AB}}_{Z_{(A,B,C,D,I,J,K,L,M,N)}} + \underbrace{|10\rangle_{EF}|01\rangle_{AB}}_{Z_{(E,F,G,H,I,J,K,L,M,N)}}, \quad (66)$$

when we apply the REM manipulations detailed in Section III-D. Hence, $|\Psi\rangle_{P7}$ of Eq. (66) becomes the final state of

$$|\Psi\rangle_{Pf} = (|00\rangle_{AF} + |11\rangle_{AF})(|00\rangle_{BE} + |11\rangle_{BE}) \quad (67)$$

B. $N = 2$ hops and $M = 2$ pairs

Let us now investigate the encoding process of an example presented in Fig. 7(b), where two pairs of entangled qubits are distributed across the network supporting $M = 2$ source-target user-pairs connected via an $N = 2$-hop back-bone with the aid of 8 pairs of entangled qubits. The encoding/decoding processes are summarised in Table II, which includes eight phases, which include an extra phase, namely Phase 2, compared to the encoding/decoding processes of the system having $N = 1$, which was detailed in Table I.

Phases	LQNC$_{(N=2,M=2)}$ Operations
1:	CON$^{A}_{C->D}$ at S_1 and R_1, CON$^{E}_{G->H}$ at S_2 and R_1
2:	CON$^{J_1}_{I_2->J_2}$ at R_2 and R_3, REM$_{J_1->I_1}$ at R_1 and R_2
3:	ADD$^{D,H}_{I_1->J_2}$ at R_1 and R_3
4:	FANOUT$^{J_2}_{K->L,M->N}$ at R_3, T_1 and T_2
5:	CNOT^{N,F} at T_1, CNOT^{L,B} at T_2
6:	REM$_{N->J_2}$ at R_3 and T_1, REM$_{L->J_2}$ at R_3 and T_2
7:	REMADD$_{J_2->D,H}$ at R_1 and R_2
8:	REM$_{D->A}$ at R_1 and S_1, REM$_{H->E}$ at R_1 and S_2

TABLE II: Encoding process of LQNC associated with the system portrayed in Fig. 7(b).

Accordingly, as seen in Fig. 7(b) the system has an initial state of

$$|\Psi\rangle_{init} = |MN\rangle|KL\rangle|I_1J_1\rangle|I_2J_2\rangle|GH\rangle|EF\rangle|CD\rangle|AB\rangle. \quad (68)$$

When encountering the phases listed in Table II, the states of the system are changed as follows.

1) Phase 1 of LQNC$_{(N=2,M=2)}$: is the same as Step 1 in Table I, hence the state after the step becomes

$$|\Psi\rangle_{P1} = |MN\rangle|KL\rangle|I_1J_1\rangle|I_2J_2\rangle \underbrace{\frac{1}{\sqrt{2}}\left(|000\rangle_{EFH} \underbrace{+|111\rangle_{EFH}}_{Z_{(E,F,G,H)}}\right)}_{\text{From CON}^{E}_{G->H}} \underbrace{\frac{1}{\sqrt{2}}\left(|000\rangle_{ABD} \underbrace{+|111\rangle_{ABD}}_{Z_{(A,B,C,D)}}\right)}_{\text{From CON}^{A}_{C->D}}. \quad (69)$$

2) Phase 2 of LQNC$_{(N=2,M=2)}$: is to connect two pairs in the backbone so that $|I_1J_1\rangle|I_2J_2\rangle$ is transformed into $|I_1J_2\rangle$. As detailed in Table II, by applying the CON operation detailed in Section III-A and then the REM operation presented in Section III-D, to $|\Psi\rangle_{P1}$ of Eq. (69), we can arrive at

$$|\Psi\rangle_{P1} = \frac{1}{2\sqrt{2}}|MN\rangle|KL\rangle \left(|00\rangle_{I_1J_2} + \underbrace{|11\rangle_{I_1J_2}}_{Z_{(I_1,J_1,I_2,J_2)}}\right) \left(|000\rangle_{EFH} \underbrace{+|111\rangle_{EFH}}_{Z_{(E,F,G,H)}}\right) \left(|000\rangle_{ABD} \underbrace{+|111\rangle_{ABD}}_{Z_{(A,B,C,D)}}\right). \quad (70)$$

3) Phase 3-to-Phase 8 of LQNC$_{(N=2,M=2)}$: It can be assumed that $|I_1J_2\rangle$ in Table II plays a role similar to that of $|IJ\rangle$ in Table I. As a result, Phase 3 to Phase 8 of Table II is equivalent to Phase 2 to Phase 7 of Table I. Hence, by applying the results obtained throughout Phase 2 to Phase 7, which are detailed in Section IV-A, the state of the system after Phase 8 of Table II may be represented as

$$|\Psi\rangle_{P7} = |00\rangle_{EF}|00\rangle_{AB} + \underbrace{|11\rangle_{AB}|11\rangle_{EF}}_{Z_{(E,F,G,H,A,B,C,D)}} + \underbrace{|01\rangle_{EF}|10\rangle_{AB}}_{Z_{(A,B,C,D,I_1,J_1,I_2,J_2K,L,M,N)}} + \underbrace{|10\rangle_{EF}|01\rangle_{AB}}_{Z_{(E,F,G,H,I_1,J_1,I_2,J_2,K,L,M,N)}}, \quad (71)$$

which leads to the final state to be

$$|\Psi\rangle_{final} = |AF\rangle|BE\rangle. \quad (72)$$

C. N-hops and $M = 2$ users

The formulation on the system having two hops can be generalised for a larger system having an arbitrary number of N hops, where the encoding/decoding processes are presented in Table III.

Phases	LQNC$_{(N,M=2)}$ Operations
1:	CON$^{A}_{C->D}$ at S_1 and R_1, CON$^{E}_{G->H}$ at S_2 and R_1
2:	CON$^{J_1}_{I_2->J_2}$ at R_2 and R_3 REM$_{J_1->I_1}$ at R_1 and R_2 ... ... CON$^{J_{N-1}}_{I_N->J_N}$ at R_N and R_{N+1} REM$_{J_{N-1}->I_{N-1}}$ at R_{N-1} and R_N
3:	ADD$^{D,H}_{I_1->J_2}$ at R_1 and R_3
4:	FANOUT$^{J_2}_{K->L,M->N}$ at R_3, T_1 and T_2
5:	CNOT^{N,F} at T_1, CNOT^{L,B} at T_2
6:	REM$_{N->J_2}$ at R_3 and T_1, REM$_{L->J_2}$ at R_3 and T_2
7:	REMADD$_{J_2->D,H}$ at R_1 and R_2
8:	REM$_{D->A}$ at R_1 and S_1, REM$_{H->E}$ at R_1 and S_2

TABLE III: Encoding process of LQNC having N hops and supporting $M = 2$ users.

Then, the final state of the system having N hops and supporting $M = 2$ users becomes

$$\begin{aligned}|\Psi\rangle_{final} &= |00\rangle_{EF}|00\rangle_{AB} + \\ &\underbrace{|11\rangle_{AB}|11\rangle_{EF}}_{Z_{(E,F,G,H,A,B,C,D)}} + \\ &\underbrace{|01\rangle_{EF}|10\rangle_{AB}}_{Z_{(A,B,C,D,I_1,J_1,I_2,J_2,\ldots,I_N,J_N,K,L,M,N)}} + \\ &\underbrace{|10\rangle_{EF}|01\rangle_{AB}}_{Z_{(E,F,G,H,I_1,J_1,I_2,J_2,\ldots,I_N,J_N,K,L,M,N)}}. \quad (73)\end{aligned}$$

V. M PAIRS OF SOURCE-AND-TARGET USERS IN N-HOP SYSTEMS

We use an example in order to illustrate the encoding/decoding process associated with the general system supporting M pairs of source-and-target users connected via an N-hop backbone link. Hence, let us now investigate the encoding/decoding processes of the system presented in Fig. 7(c), where $M = 4$ pairs of entangled qubits are distributed across the network having an $N = 2$-hop back bone. As readily seen in Fig. 7(c), $(3M + MN/2) = 16$ pairs of entangled qubits are involved in the encoding/decoding processes, which include the eight phases summarised in Table IV. Then, the encoding/decoding processes are generalised for covering the system having N hops and supporting M source-target user-pairs, where N and M can be arbitrarily large.

A. Encoding/decoding processes for systems having $N = 2$ hops and $M = 4$ pairs of users

According to the phases listed in Table IV, the system has an initial state of

$$\begin{aligned}|\Psi\rangle_{init} &= |M_2N_2\rangle|K_2L_2\rangle|M_1N_1\rangle|K_1L_1\rangle|I_{22}J_{22}\rangle|I_{21}J_{21}\rangle \\ &\quad |I_{12}J_{12}\rangle|I_{11}J_{11}\rangle|G_2H_2\rangle|E_2F_2\rangle|C_2D_2\rangle|A_2B_2\rangle \\ &\quad |G_1H_1\rangle|E_1F_1\rangle|C_1D_1\rangle|A_1B_1\rangle. \quad (74)\end{aligned}$$

Phases	QNC$_{(N=2,M=4)}$ Operations
1:	CON$^{A_1}_{C_1->D_1}$ at S_1 and R_1 CON$^{A_2}_{C_2->D_2}$ at S_2 and R_1 CON$^{E_1}_{G_1->H_1}$ at S_4 and R_1 CON$^{E_2}_{G_2->H_2}$ at S_3 and R_1
2:	CON$^{J_{11}}_{I_{12}->J_{12}}$ at R_2 and R_3 REM$_{J_{11}->I_{11}}$ at R_1 and R_2 CON$^{J_{21}}_{I_{22}->J_{22}}$ at R_2 and R_3 REM$_{J_{21}->I_{21}}$ at R_1 and R_2
3:	ADD$^{D_1,H_1}_{I_{11}->J_{12}}$, ADD$^{D_2,H_2}_{I_{21}->J_{22}}$ at R_1 and R_2
4:	FAN$^{J_{12}}_{K_1->L_1,M_1->N_1}$ at R_2,T_1 and T_2 , FAN$^{J_{22}}_{K_2->L_2,M_2->N_2}$ at R_2, T_3 and T_4
5:	CNOT^{N_1,F_1} at T_4 CNOT^{N_2,F_2} at T_3 CNOT^{L_1,B_1} at T_1 CNOT^{L_2,B_2} at T_2
6:	REM$_{N_1->J_1}$ at R_2 and T_4 REM$_{N_2->J_2}$ at R_2 and T_3 REM$_{L_1->J_1}$ at R_2 and T_1 REM$_{L_2->J_2}$ at R_2 and T_2
7:	REMADD$_{J_{12}->D_1,H_1}$ and REMADD$_{J_{22}->D_2,H_2}$ at R_1 and R_3
8	REM$_{D_1->A_1}$ at R_1 and S_1 REM$_{D_2->A_2}$ at R_1 and S_2 REM$_{H_1->E_1}$ at R_1 and S_4 REM$_{H_2->E_2}$ at R_1 and S_3

TABLE IV: Encoding process of the LQNC$_{(N=2,M=4)}$ portrayed in Fig. 7(c).

1) Phase 1 of QNC$_{(N=2,M=4)}$: is to carry out the following operations

- CON$^{A_1}_{C_1->D_1}$ at S_1 and R_1,
- CON$^{A_2}_{C_2->D_2}$ at S_2 and R_1,
- CON$^{E_1}_{G_1->H_1}$ at S_4 and R_1,
- CON$^{E_2}_{G_2->H_2}$ at S_3 and R_1,

which transform $|\Psi\rangle_{init}$ of Eq. (74) to

$$\begin{aligned}|\Psi\rangle_{P1} &= |M_2N_2\rangle|K_2L_2\rangle|M_1N_1\rangle|K_1L_1\rangle|I_{22}J_{22}\rangle|I_{21}J_{21}\rangle|I_{12}J_{12}\rangle \\ &\quad |I_{11}J_{11}\rangle|E_2F_2H_2\rangle|A_2B_2D_2\rangle|E_1F_1H_1\rangle|A_1B_1D_1\rangle, \quad (75)\end{aligned}$$

where the result of the CON operation detailed in Section III-A is applied.

2) Phase 2 of QNC$_{(N=2,M=4)}$: is to perform the following operations

- CON$^{J_{11}}_{I_{12}->J_{12}}$ at R_2 and R_3,
- REM$_{J_{11}->I_{11}}$ at R_1 and R_2,
- CON$^{J_{21}}_{I_{22}->J_{22}}$ at R_2 and R_3,
- REM$_{J_{21}->I_{21}}$ at R_1 and R_2,

in order evolve the system's state to

$$\begin{aligned}|\Psi\rangle_{P2} &= |M_2N_2\rangle|K_2L_2\rangle|M_1N_1\rangle|K_1L_1\rangle|I_{21}J_{22}\rangle|I_{11}J_{12}\rangle \\ &\quad |E_2F_2H_2\rangle|A_2B_2D_2\rangle|E_1F_1H_1\rangle|A_1B_1D_1\rangle. \quad (76)\end{aligned}$$

3) Phase 3 of QNC$_{(N=2,M=4)}$: is to execute the following operations

- ADD$^{D_1,H_1}_{I_{11}->J_{12}}$ at R_1 and R_2;
- ADD$^{D_2,H_2}_{I_{21}->J_{22}}$ at R_1 and R_2.

As a result, the system's state evolves from $|\Psi\rangle_{P2}$ of Eq. (76) to

$$|\Psi\rangle_{P2} = |M_2N_2\rangle|K_2L_2\rangle|M_1N_1\rangle|K_1L_1\rangle|\Sigma_{32}\rangle|\Sigma_{31}\rangle, \quad (77)$$

where $|\Sigma_{31}\rangle$ and $|\Sigma_{32}\rangle$ are in the following forms

$$\begin{aligned}|\Sigma_{31}\rangle &= |000\rangle_{E_1F_1H_1}|000\rangle_{A_1B_1D_1}|0\rangle_{J_{12}} + \\ &\underbrace{|111\rangle_{A_1B_1D_1}|111\rangle_{E_1F_1H_1}}_{Z_{(E_1,F_1,G_1,H_1,A_1,B_1,C_1,D_1)}}|0\rangle_{J_{12}} + \\ &\underbrace{|000\rangle_{E_1F_1H_1}|111\rangle_{A_1B_1D_1}}_{Z_{(A_1,B_1,C_1,D_1)}}\underbrace{|1\rangle_J}_{Z_{(I_{11},J_{11},I_{12},J_{12})}} + \\ &\underbrace{|111\rangle_{E_1F_1H_1}|000\rangle_{A_1B_1D_1}}_{Z_{(E_1,F_1,G_1,H_1)}}\underbrace{|1\rangle_J}_{Z_{(I_{11},J_{11},I_{12},J_{12})}}, \quad (78)\end{aligned}$$

$$\begin{aligned}|\Sigma_{32}\rangle &= |000\rangle_{E_2F_2H_2}|000\rangle_{A_2B_2D_2}|0\rangle_{J_{22}} + \\ &\underbrace{|111\rangle_{A_2B_2D_2}|111\rangle_{E_2F_2H_2}}_{Z_{(E_2,F_2,G_2,H_2,A_2,B_2,C_2,D_2)}}|0\rangle_{J_{22}} + \\ &\underbrace{|000\rangle_{E_2F_2H_2}|111\rangle_{A_2B_2D_2}}_{Z_{(A_2,B_2,C_2,D_2)}}\underbrace{|1\rangle_J}_{Z_{(I_{11},J_{11},I_{12},J_{12})}} + \\ &\underbrace{|111\rangle_{E_2F_2H_2}|000\rangle_{A_2B_2D_2}}_{Z_{(E_2,F_2,G_2,H_2)}}\underbrace{|1\rangle_J}_{Z_{(I_{21},J_{21},I_{22},J_{22})}}, \quad (79)\end{aligned}$$

where for the sake of presentation, the indices i, j of $|\Sigma_{ij}\rangle$ are used for indicating the j^{th} intermediate term in the i^{th} phase.

4) Phase 4 of QNC$_{(N=2,M=4)}$: proceeds by carrying out the following operations

- FAN$^{J_{12}}_{K_1->L_1,M_1->N_1}$ at R_2,T_1 and T_2;
- FAN$^{J_{22}}_{K_2->L_2,M_2->N_2}$ at R_2, T_3 and T_4.

By applying the results of the processes detailed in Section IV-A3, the state obtained becomes

$$|\Psi\rangle_{P4} = |\Sigma_{42}\rangle|\Sigma_{41}\rangle, \quad (80)$$

where $|\Pi_{41}\rangle$ and $|\Pi_{42}\rangle$ can be represented by

$$\begin{aligned}|\Sigma_{41}\rangle &= |000\rangle_{E_1F_1H_1}|000\rangle_{A_1B_1D_1}|000\rangle_{J_{22}N_1L_1} + \\ &\underbrace{|111\rangle_{A_1B_1D_1}|111\rangle_{E_1F_1H_1}}_{Z_{(E_1,F_1,G_1,H_1,A_1,B_1,C_1,D_1)}}|000\rangle_{J_{12}N_1L_1} + \\ &\underbrace{|000\rangle_{E_1F_1H_1}|111\rangle_{A_1B_1D_1}}_{Z_{(A_1,B_1,C_1,D_1)}}\underbrace{|111\rangle_{J_{22}N_1L_1}}_{Z_{(I_{11},J_{11},I_{12},J_{12},K_1,L_1,M_1,N_1)}} \\ &\underbrace{|111\rangle_{E_1F_1H_1}|000\rangle_{A_1B_1D_1}}_{Z_{(E_1,F_1,G_1,H_1)}}\underbrace{|111\rangle_{J_{22}N_1L_1}}_{Z_{(I_{11},J_{11},I_{12},J_{12},K_1,L_1,M_1,N_1)}} \quad (81)\end{aligned}$$

$$\begin{aligned}|\Sigma_{42}\rangle &= |000\rangle_{E_2F_2H_2}|000\rangle_{A_2B_2D_2}|000\rangle_{J_{22}N_2L_2} + \\ &\underbrace{|111\rangle_{A_2B_2D_2}|111\rangle_{E_2F_2H_2}}_{Z_{(E_2,F_2,G_2,H_2,A_2,B_2,C_2,D_2)}}|000\rangle_{J_{22}N_2L_2} + \\ &\underbrace{|000\rangle_{E_2F_2H_2}|111\rangle_{A_2B_2D_2}}_{Z_{(A_2,B_2,C_2,D_2)}}\underbrace{|111\rangle_{J_{22}N_2L_2}}_{Z_{(I_{11},J_{11},I_{12},J_{12},K_2,L_2,M_2,N_2)}} + \\ &\underbrace{|111\rangle_{E_2F_2H_2}|000\rangle_{A_2B_2D_2}}_{Z_{(E_2,F_2,G_2,H_2)}}\underbrace{|111\rangle_{J_{22}N_2L_2}}_{Z_{(I_{11},J_{11},I_{22},J_{12},K_2,L_2,M_2,N_2)}} \quad (82)\end{aligned}$$

5) Phase 5 of QNC$_{(N=2,M=4)}$: proceeds by carrying out the following operations

- CNOT^{N_1,F_1} at T_4 ;
- CNOT^{N_2,F_2} at T_3 ;
- CNOT^{L_1,B_1} at T_1 ;
- CNOT^{L_2,B_2} at T_2 ,

which leads to the following state

$$|\Psi\rangle_{P5} = |\Sigma_{52}\rangle|\Sigma_{51}\rangle, \quad (83)$$

where the terms $|\Sigma_{52}\rangle$ and $|\Sigma_{51}\rangle$ are :

$$\begin{aligned}|\Sigma_{51}\rangle &= |000\rangle_{E_1F_1H_1}|000\rangle_{A_1B_1D_1}|000\rangle_{J_{12}N_1L_1} + \\ &\underbrace{|111\rangle_{A_1B_1D_1}|111\rangle_{E_1F_1H_1}}_{Z_{(E_1,F_1,G_1,H_1,A_1,B_1,C_1,D_1)}}|000\rangle_{J_{12}N_1L_1} + \\ &\underbrace{|010\rangle_{E_1F_1H_1}|101\rangle_{A_1B_1D_1}}_{Z_{(A_1,B_1,C_1,D_1)}}\underbrace{|111\rangle_{J_{12}N_1L_1}}_{Z_{(I_{11},J_{11},I_{12},J_{12},K_1,L_1,M_1,N_1)}} + \\ &\underbrace{|101\rangle_{E_1F_1H_1}|010\rangle_{A_1B_1D_1}}_{Z_{(E_1,F_1,G_1,H_1)}}\underbrace{|111\rangle_{J_{12}N_1L_1}}_{Z_{(I_{11},J_{11},I_{12},J_{12},K_1,L_1,M_1,N_1)}} \quad (84)\end{aligned}$$

$$\begin{aligned}|\Sigma_{52}\rangle &= |000\rangle_{E_2F_2H_2}|000\rangle_{A_2B_2D_2}|000\rangle_{J_{22}N_2L_2} + \\ &\underbrace{|111\rangle_{A_2B_2D_2}|111\rangle_{E_2F_2H_2}}_{Z_{(E_2,F_2,G_2,H_2,A_2,B_2,C_2,D_2)}}|000\rangle_{J_{22}N_2L_2} + \\ &\underbrace{|010\rangle_{E_2F_2H_2}|101\rangle_{A_2B_2D_2}}_{Z_{(A_2,B_2,C_2,D_2)}}\underbrace{|111\rangle_{J_{22}N_2L_2}}_{Z_{(I_{11},J_{11},I_{12},J_{12},K_2,L_2,M_2,N_2)}} + \\ &\underbrace{|101\rangle_{E_2F_2H_2}|010\rangle_{A_2B_2D_2}}_{Z_{(E_2,F_2,G_2,H_2)}}\underbrace{|111\rangle_{J_{22}N_2L_2}}_{Z_{(I_{11},J_{11},I_{22},J_{12},K_2,L_2,M_2,N_2)}} \quad (85)\end{aligned}$$

6) Phase 6 of QNC$_{(N=2,M=4)}$: is performed by carrying out the following operations

- REM$_{N_1->J_{12}}$ at R_3 and T_4;
- REM$_{N_2->J_{22}}$ at R_3 and T_3;
- REM$_{L_1->J_{12}}$ at R_3 and T_1;
- REM$_{L_2->J_{22}}$ at R_3 and T_2.

As a result, the system state after Phase 6 of Table IV becomes

$$|\Psi\rangle_{P6} = |\Sigma_{62}\rangle|\Sigma_{61}\rangle, \quad (86)$$

where the terms $|\Sigma_{61}\rangle$ and $|\Sigma_{62}\rangle$ are represented by

$$\begin{aligned}|\Sigma_{61}\rangle &= |000\rangle_{E_1F_1H_1}|000\rangle_{A_1B_1D_1}|0\rangle_{J_{12}} + \\ &\underbrace{|111\rangle_{A_1B_1D_1}|111\rangle_{E_1F_1H_1}}_{Z_{(E_1,F_1,G_1,H_1,A_1,B_1,C_1,D_1)}}|0\rangle_{J_{12}} + \\ &\underbrace{|010\rangle_{E_1F_1H_1}|101\rangle_{A_1B_1D_1}}_{Z_{(A_1,B_1,C_1,D_1)}}\underbrace{|1\rangle_{J_{12}}}_{Z_{(I_{11},J_{11},I_{12},J_{12},K_1,L_1,M_1,N_1)}} + \\ &\underbrace{|101\rangle_{E_1F_1H_1}|010\rangle_{A_1B_1D_1}}_{Z_{(E_1,F_1,G_1,H_1)}}\underbrace{|1\rangle_{J_{12}}}_{Z_{(I_{11},J_{11},I_{12},J_{12},K_1,L_1,M_1,N_1)}} \quad (87)\end{aligned}$$

$$\begin{aligned}|\Sigma_{62}\rangle &= |000\rangle_{E_2F_2H_2}|000\rangle_{A_2B_2D_2}|0\rangle_{J_{22}} + \\ &\underbrace{|111\rangle_{A_2B_2D_2}|111\rangle_{E_2F_2H_2}}_{Z_{(E_2,F_2,G_2,H_2,A_2,B_2,C_2,D_2)}}|0\rangle_{J_{22}} + \\ &\underbrace{|010\rangle_{E_2F_2H_2}|101\rangle_{A_2B_2D_2}}_{Z_{(A_2,B_2,C_2,D_2)}}\underbrace{|1\rangle_{J_{22}}}_{Z_{(I_{11},J_{11},I_{12},J_{12},K_2,L_2,M_2,N_2)}} + \\ &\underbrace{|101\rangle_{E_2F_2H_2}|010\rangle_{A_2B_2D_2}}_{Z_{(E_2,F_2,G_2,H_2)}}\underbrace{|1\rangle_{J_{22}}}_{Z_{(I_{11},J_{11},I_{22},J_{12},K_2,L_2,M_2,N_2)}} \quad (88)\end{aligned}$$

7) Phase 7 of QNC$_{(N=2,M=4)}$: proceeds by performing the following operations

- REMADD$_{J_{12}->D_1,H_1}$ at R_1 and R_3;
- REMADD$_{J_{22}->D_2,H_2}$ at R_1 and R_3.

Accordingly, we have the following system state

$$|\Psi\rangle_{P7} = |\Sigma_{72}\rangle|\Sigma_{71}\rangle, \quad (89)$$

where the terms $|\Sigma_{71}\rangle$ and $|\Sigma_{72}\rangle$ are represented by

$$\begin{aligned}|\Sigma_{71}\rangle = & |000\rangle_{E_1F_1H_1}|000\rangle_{A_1B_1D_1} + \\ & \underbrace{|111\rangle_{A_1B_1D_1}|111\rangle_{E_1F_1H_1}}_{Z_{(E_1,F_1,G_1,H_1,A_1,B_1,C_1,D_1)}} + \\ & \underbrace{|010\rangle_{E_1F_1H_1}|101\rangle_{A_1B_1D_1}}_{Z_{(A_1,B_1,C_1,D_1,I_{11},J_{11},I_{12},J_{12},K_1,L_1,M_1,N_1)}} + \\ & \underbrace{|101\rangle_{E_1F_1H_1}|010\rangle_{A_1B_1D_1}}_{Z_{(E_1,F_1,G_1,H_1,I_{11},J_{11},I_{12},J_{12},K_1,L_1,M_1,N_1)}}, \quad (90)\end{aligned}$$

$$\begin{aligned}|\Sigma_{72}\rangle = & |000\rangle_{E_2F_2H_2}|000\rangle_{A_2B_2D_2} + \\ & \underbrace{|111\rangle_{A_2B_2D_2}|111\rangle_{E_2F_2H_2}}_{Z_{(E_2,F_2,G_2,H_2,A_2,B_2,C_2,D_2)}} + \\ & \underbrace{|010\rangle_{E_2F_2H_2}|101\rangle_{A_2B_2D_2}}_{Z_{(A_2,B_2,C_2,D_2,I_{11},J_{11},I_{12},J_{12},K_2,L_2,M_2,N_2)}} + \\ & \underbrace{|101\rangle_{E_2F_2H_2}|010\rangle_{A_2B_2D_2}}_{Z_{(E_2,F_2,G_2,H_2,I_{11},J_{11},I_{22},J_{12},K_2,L_2,M_2,N_2)}}. \quad (91)\end{aligned}$$

8) Phase 8 of QNC$_{(N=2,M=4)}$: proceeds by carrying out the following operations

- REM$_{D_1->A_1}$ at R_1 and S_1;
- REM$_{D_2->A_2}$ at R_1 and S_2;
- REM$_{H_1->E_1}$ at R_1 and S_4;
- REM$_{H_2->E_2}$ at R_1 and S_3.

As a result, the final state of the system is as follows

$$|\Psi\rangle_{final} = |\Sigma_{82}\rangle|\Sigma_{81}\rangle, \quad (92)$$

where the terms $|\Sigma_{81}\rangle$ and $|\Sigma_{82}\rangle$ are represented by

$$\begin{aligned}|\Sigma_{81}\rangle = & |00\rangle_{E_1F_1}|00\rangle_{A_1B_1} + \\ & \underbrace{|11\rangle_{A_1B_1}|11\rangle_{E_1F_1}}_{Z_{(E_1,F_1,G_1,H_1,A_1,B_1,C_1,D_1)}} + \\ & \underbrace{|01\rangle_{E_1F_1}|10\rangle_{A_1B_1}}_{Z_{(A_1,B_1,C_1,D_1,I_{11},J_{11},I_{12},J_{12},K_1,L_1,M_1,N_1)}} + \\ & \underbrace{|10\rangle_{E_1F_1}|01\rangle_{A_1B_1}}_{Z_{(E_1,F_1,G_1,H_1,I_{11},J_{11},I_{12},J_{12},K_1,L_1,M_1,N_1)}}, \quad (93)\end{aligned}$$

$$\begin{aligned}|\Sigma_{82}\rangle = & |00\rangle_{E_2F_2}|00\rangle_{A_2B_2} + \\ & \underbrace{|11\rangle_{A_2B_2}|11\rangle_{E_2F_2}}_{Z_{(E_2,F_2,G_2,H_2,A_2,B_2,C_2,D_2)}} + \\ & \underbrace{|01\rangle_{E_2F_2}|10\rangle_{A_2B_2}}_{Z_{(A_2,B_2,C_2,D_2,I_{11},J_{11},I_{12},J_{12},K_2,L_2,M_2,N_2)}} + \\ & \underbrace{|10\rangle_{E_2F_2}|01\rangle_{A_2B_2}}_{Z_{(E_2,F_2,G_2,H_2,I_{11},J_{11},I_{22},J_{12},K_2,L_2,M_2,N_2)}}. \quad (94)\end{aligned}$$

As a result, we have the corresponding final state :

$$|\Psi\rangle_{final} = |A_1F_1\rangle|A_2F_2\rangle|B_1E1\rangle|B_2E_2\rangle. \quad (95)$$

B. Large-scale networks having N-hops and supporting M-pairs

Based on the LQNC$_{(N=2,M=4)}$ system detailed Section V-A, we can now formulate the general system having N-hops and supporting M-pairs of entangled qubits, which has an initial state of

$$\begin{aligned}|\Psi\rangle_{init} = & |M_{\frac{M}{2}}N_{\frac{M}{2}}\rangle|K_{\frac{M}{2}}L_{\frac{M}{2}}\rangle\cdots|M_1N_1\rangle|K_1L_1\rangle \\ & |I_{\frac{M}{2}N}J_{\frac{M}{2}N}\rangle\cdots|I_{\frac{M}{2}1}J_{\frac{M}{2}1}\rangle\cdots\cdots \\ & |I_{1N}J_{1N}\rangle\cdots|I_{11}J_{11}\rangle \\ & |G_{\frac{M}{2}}H_{\frac{M}{2}}\rangle|E_{\frac{M}{2}}F_{\frac{M}{2}}\rangle|C_{\frac{M}{2}}D_{\frac{M}{2}}\rangle|A_{\frac{M}{2}}B_{\frac{M}{2}}\rangle\cdots \\ & |G_1H_1\rangle|E_1F_1\rangle|C_1D_1\rangle|A_1B_1\rangle. \quad (96)\end{aligned}$$

Given the results of Section V-A, we can have the final state of LQNC$_{(N,M)}$

$$|\Psi\rangle_{final} = |\Sigma_{8\frac{M}{2}}\rangle\cdots|\Sigma_{81}\rangle, \quad (97)$$

where the terms $|\Sigma_{8i}\rangle$, $i=[1,\ldots,\frac{M}{2}]$ are represented by

$$\begin{aligned}|\Sigma_{8i}\rangle = & |00\rangle_{E_iF_i}|00\rangle_{A_iB_i} + \\ & \underbrace{|11\rangle_{A_iB_i}|11\rangle_{E_iF_i}}_{Z_{(E_i,F_i,G_i,H_i,A_i,B_i,C_i,D_i)}} + \\ & \underbrace{|01\rangle_{E_iF_i}|10\rangle_{A_iB_i}}_{Z_{(A_i,B_i,C_i,D_i,I_{i1},J_{i1},\cdots,I_{iN},J_{iN},K_i,L_i,M_i,N_i)}} + \\ & \underbrace{|10\rangle_{E_iF_i}|01\rangle_{A_iB_i}}_{Z_{(E_i,F_i,G_i,H_i,I_{i1},J_{i1},\cdots,I_{iN},J_{iN},K_i,L_i,M_i,N_i)}}. \quad (98)\end{aligned}$$

Hence, final state $|\Psi\rangle_{final}$ of Eq. (97) is equivalent to

$$|\Psi\rangle_{final} = |A_{\frac{M}{2}}F_{\frac{M}{2}}\rangle|B_{\frac{M}{2}}E_{\frac{M}{2}}\rangle\cdots|A_1F_1\rangle|B_1E_1\rangle. \quad (99)$$

VI. Entanglement Swapping

Let us now consider the quantum domain network portrayed in Fig. 8 having three nodes, namely source s, relay r and target t. The ES protocol is invoked for establishing the entanglement between two far-end qubits, namely $|A\rangle$ and $|D\rangle$. The realisation of the ES protocol can be divided into the two phases detailed in Table V.

Phases	Entanglement Swapping Protocol
1	CON$^B_{C->D}$
2	REM$_{B->A}$

TABLE V: ES protocol illustrated in Fig. 8.

The ES-based system of Fig. 8 may have an initial state of

$$|\Psi\rangle_{init} = \frac{1}{2}\left(|00\rangle_{AB} + |11\rangle_{AB}\right)\left(|00\rangle_{CD} + |11\rangle_{CD}\right). \quad (100)$$

Following the operation of CON$^B_{C->D}$ in Phase 1 of Table V, the system's state becomes

$$|\Psi\rangle_{ES1} = \frac{1}{\sqrt{2}}|000\rangle_{ABD} + \underbrace{\frac{1}{\sqrt{2}}|111\rangle_{ABD}}_{Z_{(A,B,C,D)}}, \quad (101)$$

where the principles of CON$^B_{C->D}$ are detailed in Section III-A.

Following Phase 2 of Table V, where the operation $\text{REM}_{B->A}$ is carried out, the system's state evolves to

$$|\Psi\rangle_{ES2} = \frac{1}{\sqrt{2}}|00\rangle_{AD} \underbrace{+\frac{1}{\sqrt{2}}|11\rangle_{AD}}_{Z_{(A,B,C,D)}}, \quad (102)$$

where the details of $\text{REM}_{B->A}$ are illustrated in Section III-D. The probability of having no errors in state $|\Psi\rangle_{ES2}$ of Eq. (102) is equal to the probability of actually ending up with no errors caused by the combined error $Z_{(A,B,C,D)}$ as a benefit of the errors cancelling each other. In ES-based systems having $(N+2)$ hops, where $|AB\rangle$ and $|CD\rangle$ are connected by an N-hop backbone link constructed from N pairs of entangled qubits, namely $|I_1J_1\rangle \cdots |I_NJ_N\rangle$, the phases in Table V are repeated, hence resulting in the final state of

$$|\Psi\rangle_{ESf} = \frac{1}{\sqrt{2}}|00\rangle_{AD} \underbrace{+\frac{1}{\sqrt{2}}|11\rangle_{AD}}_{Z_{(A,B,I_1,J_1,\ldots,I_N,J_N,C,D)}}. \quad (103)$$

Accordingly, the probability of having no errors then can be generated from Eq. (103) for some examples, as listed in Table VI. It should be noted that the $P^{ES}_{0(M=1)}$ of Table VI is valid for the system supporting an $M=1$ source-target user-pair. Hence, for the system supporting an arbitrary number of M pairs the corresponding probability is calculated by

$$P^{ES}_{0(M)} = \left[P^{ES}_{0(M=1)}\right]^M. \quad (104)$$

ES (N)	Probability of having no errors $(P^{ES}_{0(M=1)})$
$N=1$	$3F(1-F)^2+F^3$
$N=2$	$(1-F)^4+6F^2(1-F)^2+F^4$
$N=3$	$5F(1-F)^4+10F^3(1-F)^2+F^5$
$N=4$	$(1-F)^6+15F^2(1-F)^4+15F^4(1-F)^2+F^6$

TABLE VI: Probabilities of having no errors in the ES-based systems associated with $N=[1,2,3,4]$

VII. Performance Comparisons

A. Error pattern

Let us recall the encoding example of the $\text{QNC}_{(N=1,M=2)}$ from Section IV-A, where the final state $|\Psi\rangle_{P7}$ of Eq. (66) contains potential Z-errors, namely

$$\begin{aligned} Z^1 &= Z_{(E,F,G,H,A,B,C,D)} \\ Z^2 &= Z_{(A,B,C,D,I,J,K,L,M,N)} \\ Z^3 &= Z_{(E,F,G,H,I,J,K,L,M,N)}. \end{aligned} \quad (105)$$

Based on the Z-error conditions of Eq. (105), we may determine the no-error/error patterns associated with every possible Z-errors imposed on each of the $Y = 3M + MN/2 = 7$ pairs of entangled qubits. As a result, focusing on the no-error pattern, the fidelity of the system's final state is equivalent to the probability of having no-error in the final state $|\Psi\rangle_{P7}$ of Eq. (66)

$$\begin{aligned} P_0 = {} & F^7 + 5F^5(1-F)^2 + 12F^4(1-F)^3 + 7F^3(1-F)^4 \\ & + 4F^2(1-F)^5 + 3F(1-F)^6, \end{aligned} \quad (106)$$

where F is the fidelity of an entangled pair in the network detailed in Section II-B. For the ease of explanation, we assume all the pairs in the system to have the same fidelity F. However, even if each pair in the system has different fidelity, the same method can be used for evaluating the final state's fidelity.

For the general case of $\text{LQNC}_{(N,M)}$ having a final state presented in Eq. (97) and Eq. (98), the Z-error conditions can be similarly extracted for the sake of identifying the error/no-error patterns. As a result, in Table VII we calculated the no-error probability for several examples of LQNC systems.

LQNC (M,N)	Non-error probability (P_0^{LQNC})
$M=2, N=2$	$(1-F)^8+8F^2(1-F)^6+16F^3(1-F)^5+$ $14F^4(1-F)^4+16F^5(1-F)^3+$ $8F^6(1-F)^2+F^8$
$M=2, N=3$	$5F(1-F)^8+4F^2(1-F)^7+20F^3(1-F)^6+$ $40F^4(1-F)^5+26F^5(1-F)^4+20F^6(1-F)^3+$ $12F^7(1-F)^2+F^9$
$M=2, N=4$	$(1-F)^{10}+17F^2(1-F)^8+24F^3(1-F)^7+$ $46F^4(1-F)^6+80F^5(1-F)^5+46F^6(1-F)^4+$ $24F^7(1-F)^3+17F^8(1-F)^2+F^{10}$

TABLE VII: Probabilities of no-error-scenarios

B. Coding rate

Given a system supporting M pairs of source-target users via an N-hop backbone link, either the LQNC-based system of Fig. 9(b) or the ES-based system of Fig. 9(a) can be used by employing Y entangled pairs in the system, which are given by

$$Y_{ES} = M(2+N), \quad (107)$$

and

$$Y_{LQNC} = 3M + \frac{MN}{2}. \quad (108)$$

By comparing Y_{ES} of Eq. (107) and Y_{LQNC} of Eq. (108), it can be inferred that in order to support M pairs of source-target users ES requires more entangled pairs than LQNC, when the system has more than two hops, i. e. for $N>2$. Moreover, the term F representing the average fidelity of an entangled pairs in the initial system's state in the formulae of P_0^{ES} in Table VI and P_0^{LQNC} in Table VII becomes the most dominant term, when the value of fidelity approaches $F = F_{in} = 1$, which is inversely proportional to Y. As a result, Y_{ES} and Y_{LQNC} can be used for predicting the fidelity of both the ES-based system and of the LQNC-based system.

Considering the processes of ES and LQNC as encoding/decoding processes, let us define the coding rate in the system employing LQNC as

$$R_{LQNC} = \frac{M}{Y_{LQNC}} = \frac{2}{6+N}, \quad (109)$$

while that in the system using ES is defined by

$$R_{ES} = \frac{M}{Y_{ES}} = \frac{1}{2+N}. \quad (110)$$

It can be inferred from Eq. (109) and Eq. (110) that we have $R_{LQNC} > R_{ES}$, when the system relies on more than two

hops, $N > 2$. As a result, it is expected that in the system having $N > 2$ hops the LQNC-based protocol is able to provide a better fidelity-performance and higher coding rate.

C. Performance comparison of LQNC vs. ES

Let us assume that the average fidelity of a specific pair among the Y and M pairs before/after the encoding-and-decoding processes is F_{in} and F_{out}, respectively. Given F_{in}, we may have different fidelity-related performance metrics, as represented by

- F_{out}^{LQNC} and F_{out}^{ES} fidelity performance associated with the coding rate of R_{LQNC} and R_{ES}, which is quantified for different numbers of hops N and user-pairs M;
- $QBER$ performance reflecting the reciprocal of the fidelity of F_{out}^{LQNC} and F_{out}^{ES}, which is quantified for different numbers of hops N and user-pairs M;
- Fidelity degradation of $D_F = F_{in} - F_{out}$ characterising the reduction of the average fidelity after the encoding-and-decoding processes, which is quantified for different values of hops N and user-pairs M;
- The relative fidelity improvement I_F quantitatively reflecting the benefit of LQNC over ES, which is calculated by

$$I_F = 100\frac{F_{out}^{LQNC} - F_{out}^{ES}}{F_{out}^{ES}}. \quad (111)$$

- The normalised relative fidelity improvement I_F^N, quantifying I_F per entangled pair of qubits, which is calculated as

$$I_F^N = 100\frac{F_{out}^{LQNC} - F_{out}^{ES}}{F_{out}^{ES} Y_{LQNC}}. \quad (112)$$

In order to provide a quantitative performance comparison between ES-based and LQNC-based systems, we consider the examples listed in Table VIII.

Configurations (N, M)	LQNC (Y_{LQNC}, R_{LQNC})	ES (Y_{ES}, R_{ES})
$(2, 2)$	$(8, 0.25)$	$(8, 0.25)$
$(4, 2)$	$(10, 0.16)$	$(12, 0.2)$
$(3, 4)$	$(18, 0.22)$	$(20, 0.2)$
$(2, 8)$	$(32, 0.25)$	$(32, 0.25)$
$(4, 8)$	$(40, 0.16)$	$(48, 0.2)$
$(8, 12)$	$(84, 0.14)$	$(120, 0.1)$
$(10, 14)$	$(112, 0.125)$	$(168, 0.08)$

TABLE VIII: Comparison of LQNC-based and ES-based systems.

As seen in Fig. 10(a)-Fig. 10(c), when we have $N = 2$ and $M = 2$ leading to $Y_{ES} = Y_{LQNC} = 8$, the fidelity of the LQNC-based and of ES-based system is similar in the high-fidelity region, where $F_{in} = 1$ is approached. Increasing $N = 2$ to $N = 4$ hops while still supporting $M = 2$ pairs results in $Y_{LQNC} = 10 < Y_{ES} = 12$, which implies that we can expect to see the LQNC-based systems to outperform the ES-based systems in Fig. 10(d)-Fig. 10(f) right across the entire input fidelity range of F_{in}. This is in line with our analysis in Section VII-B.

Fig. 10(f) shows that the fidelity improvement of LQNC increases, when F_{in} decreases. This phenomenon is in agreement with the error correction trend typically found in the classical domain, since more powerful codes can correct more errors.

It is also interesting to see in Fig. 10(f) and Fig. 11(f) that the fidelity degradation, which is reminiscent of the path loss effects in classical communication, is reduced, when the input fidelity F_{in} decreases. This is because a Z-error in Eq. (98) can be cancelled out by another Z-error in the system.

In the system supporting as many as $M = 8$ pairs, the LQNC-based system always outperformed the ES-based system for $N > 2$ hops, as demonstrated in Fig. 11. The more pairs the system supports, the higher the fidelity degradation becomes and the gap between the two system's performance improvement is seen to widen.

The relative fidelity improvement of the two systems is presented in Fig. 12, where we can see that the larger the system associated with more hops and more user-pairs, the higher the improvement becomes. More specifically, the fidelity improvement plotted in Fig. 12(a) is in the range spanning from $I_F \approx 10^1$ % to $I_F \approx 10^3$ %, when the system dimension is scaled up from $(N = 3, M = 4)$ to $(N = 10, M = 14)$.

When we normalise the relative fidelity improvement to the total number Y of entangled pairs used, as detailed in Eq. (112), the normalised fidelity improvement of the LQNC-based systems over the ES-based system is increased from $I_F^N = 0.5$ % to $I_F^N = 8$ %, as seen in Fig. 12(b).

VIII. Design Guidelines and Conclusions

To summarise, the design of LQNC can be carried out using the following steps.

Step 1 requires us to partition the given complex network into fragments. Then, the more beneficial one of ES and LQNC protocol-pair may be used for converting the arbitrary structure of the fragments to the standard structure portrayed in Fig. 9.

Step 2 is used for interpreting the details of the design requirements, which may encompass the parameters characterising the LQNC system, including the number M of entangled pairs involved and the fidelity of F_{in} and F_{out}, as well as the number of available relays defining the number of hops N. **It should be noted that due to the conversion in Step 1, the fidelity of a particular entangled pair of qubits may vary throughout the network, hence the distinct error probabilities become useful.**

In Step 3, we construct the overall system architecture and determine the system's configuration based on the constraints and specifications given. Then, we proceed by constructing the specific encoding/decoding processes, which lead us to specific error patterns that can be used for predicting the system's performance.

In conclusion, we demonstrated the benefits of QNC in the context of a large-scale quantum network, termed as LQNC. The LQNC-based system is capable of providing about 10-times better fidelity-performance at a higher coding rate than that supported by ES-based systems, when considering a large-scale network.

REFERENCES

[1] R. Ahlswede, N. Cai, and R. Yeung, "Network information flow theory," in *IEEE International Symposium on Information Theory, 1998*, p. 186, Aug. 1998.

[2] R. Ahlswede, N. Cai, S.-Y. Li, and R. Yeung, "Network information flow," *IEEE Transactions on Information Theory*, vol. 46, pp. 1204 – 1216, July 2000.

[3] P. Chou and Y. Wu, "Network coding for the internet and wireless networks," *IEEE Signal Processing Magazine*, vol. 24, pp. 77 –85, Sept. 2007.

[4] E. Soljanin, "Network multicast with network coding [lecture notes]," *IEEE Signal Processing Magazine*, vol. 25, pp. 109 –112, Sep. 2008.

[5] Y. Chen and S. Kishore, "On the tradeoffs of implementing randomized network coding in multicast networks," *IEEE Transactions on Communications*, vol. 58, pp. 2107 –2115, July 2010.

[6] C. Fragouli and E. Soljanin, "Network coding fundamentals," *Foundation and Trends in Networking*, vol. 2, no. 1, pp. 1–133, 2007.

[7] R. W. Yeung and N. Cai, "Network error correction, Part I: Basic concepts and upper bounds," *Communications in Information and Systems*, vol. 6, no. 1, pp. 19–36, 2006.

[8] R. W. Yeung and N. Cai, "Network error correction, Part II: Lower bounds," *Communications in Information and Systems*, vol. 6, no. 1, pp. 37–54, 2006.

[9] M. Hayashi, K. Wama, H. Nishimura, R. Raymond, and S. Yamashita, *Quantum network coding*, vol. 4393 of *Lecture Notes in Computer Science*, pp. 610–621. Berlin: Springer-Verlag Berlin, 2007.

[10] D. Leung, J. Oppenheim, and A. Winter, "Quantum network communication-the butterfly and beyond," *IEEE Transactions on Information Theory*, vol. 56, no. 7, pp. 3478–3490, 2010.

[11] M. Mahdian and R. Bayramzadeh, "Perfect k-pair quantum network coding using superconducting qubits," *Journal of Superconductivity and Novel Magnetism*, vol. 28, no. 2, pp. 345–348, 2015.

[12] L. Jing, C. Xiu-Bo, X. Gang, Y. Yi-Xian, and L. Zong-Peng, "Perfect quantum network coding independent of classical network solutions," *Communications Letters, IEEE*, vol. 19, no. 2, pp. 115–118, 2015.

[13] T. Satoh, K. Ishizaki, S. Nagayama, and R. Van Meter, "Analysis of quantum network coding for realistic repeater networks," *Phys. Rev. A*, vol. 93, p. 032302, Mar 2016.

[14] T. Shang, X.-J. Zhao, and J.-W. Liu, "Quantum network coding based on controlled teleportation," *IEEE Communications Letters*, vol. 18, no. 5, pp. 865–868, 2014.

[15] T. Satoh, F. Le Gall, and H. Imai, "Quantum network coding for quantum repeaters," *Physical Review A*, vol. 86, no. 3, 2012.

[16] A. Jain, M. Franceschetti, and D. A. Meyer, "On quantum network coding," *Journal of Mathematical Physics*, vol. 52, no. 3, 2011.

[17] W. J. Munro, K. A. Harrison, A. M. Stephens, S. J. Devitt, and K. Nemoto, "From quantum multiplexing to high-performance quantum networking," *Nature Photonics*, vol. 4, no. 11, pp. 792–796, 2010.

[18] M. Hayashi, "Prior entanglement between senders enables perfect quantum network coding with modification," *Physical Review A*, vol. 76, no. 4, 2007.

[19] H. Kobayashi, F. Le Gall, H. Nishimura, and M. Rotteler, "Constructing quantum network coding schemes from classical nonlinear protocols," in *Information Theory Proceedings (ISIT), 2011 IEEE International Symposium on*, pp. 109–113.

[20] H. Kobayashi, F. L. Gall, H. Nishimura, and M. Rtteler, "Perfect quantum network communication protocol based on classical network coding," in *2010 IEEE International Symposium on Information Theory*, pp. 2686–2690, June 2010.

[21] H. Kobayashi, F. Le Gall, H. Nishimura, and M. Roetteler, *General Scheme for Perfect Quantum Network Coding with Free Classical Communication*, vol. 5555 of *Lecture Notes in Computer Science*, pp. 622–633. 2009.

[22] R. Pakniat, M. K. Tavassoly, and M. H. Zandi, "Entanglement swapping and teleportation based on cavity QED method using the nonlinear atom-field interaction: Cavities with a hybrid of coherent and number states," *OPTICS COMMUNICATIONS*, vol. 382, pp. 381–385, JAN 1 2017.

[23] C. H. Bennett, D. P. DiVincenzo, P. W. Shor, J. A. Smolin, B. M. Terhal, and W. K. Wootters, "Remote state preparation," *Phys. Rev. Lett.*, vol. 87, p. 077902, Jul 2001.

[24] Y.-S. Ra, H.-T. Lim, and Y.-H. Kim, "Remote preparation of three-photon entangled states via single-photon measurement," *Phys. Rev. A*, vol. 94, p. 042329, Oct 2016.

[25] H. Lu, Z. Zhang, L.-K. Chen, Z.-D. Li, C. Liu, L. Li, N.-L. Liu, X. Ma, Y.-A. Chen, and J.-W. Pan, "Secret sharing of a quantum state," *Phys. Rev. Lett.*, vol. 117, p. 030501, Jul 2016.

[26] A. Einstein, B. Podolsky, and N. Rosen, "Can quantum-mechanical description of physical reality be considered complete?," *Phys. Rev.*, vol. 47, pp. 777–780, May 1935.

[27] S. Imre, "Quantum communications: explained for communication engineers," *IEEE Communications Magazine*, vol. 51, pp. 28–35, August 2013.

[28] H. P. Yuen, "Security of quantum key distribution," *IEEE Access*, vol. 4, pp. 724–749, 2016.

[29] J.-P. Bourgoin, B. L. Higgins, N. Gigov, C. Holloway, C. J. Pugh, S. Kaiser, M. Cranmer, and T. Jennewein, "Free-space quantum key distribution to a moving receiver," *Optics Express*, vol. 23, no. 26, pp. 33437–33447, 2015.

[30] M. T. Gruneisen, M. B. Flanagan, B. A. Sickmiller, J. P. Black, K. E. Stoltenberg, and A. W. Duchane, "Modeling daytime sky access for a satellite quantum key distribution downlink," *Optics Express*, vol. 23, no. 18, pp. 23924–23934, 2015.

[31] G. Vallone, D. G. Marangon, M. Canale, I. Savorgnan, D. Bacco, M. Barbieri, S. Calimani, C. Barbieri, N. Laurenti, and P. Villoresi, "Adaptive real time selection for quantum key distribution in lossy and turbulent free-space channels," *Physical Review A*, vol. 91, no. 4, 2015.

[32] A. Carrasco-Casado, N. Denisenko, and V. Fernandez, "Correction of beam wander for a free-space quantum key distribution system operating in urban environment," *Optical Engineering*, vol. 53, no. 8, 2014.

[33] G. Vest, M. Rau, L. Fuchs, G. Corrielli, H. Weier, S. Nauerth, A. Crespi, R. Osellame, and H. Weinfurter, "Design and evaluation of a handheld quantum key distribution sender module," *IEEE Journal of Selected Topics in Quantum Electronics*, vol. 21, pp. 131–137, May 2015.

[34] M. Rau, T. Heindel, S. Unsleber, T. Braun, J. Fischer, S. Frick, S. Nauerth, C. Schneider, G. Vest, S. Reitzenstein, M. Kamp, A. Forchel, S. Hoefling, and H. Weinfurter, "Free space quantum key distribution over 500 meters using electrically driven quantum dot single-photon sources-a proof of principle experiment," *New Journal of Physics*, vol. 16, 2014.

[35] W. J. Munro, K. Azuma, K. Tamaki, and K. Nemoto, "Inside quantum repeaters," *IEEE Journal of Selected Topics in Quantum Electronics*, vol. 21, pp. 78–90, May 2015.

[36] C. Y. Chen, G. J. Zeng, F. j. Lin, Y. H. Chou, and H. C. Chao, "Quantum cryptography and its applications over the internet," *IEEE Network*, vol. 29, pp. 64–69, September 2015.

[37] A. Hellemans, "Two steps closer to a quantum internet [news]," *IEEE Spectrum*, vol. 53, pp. 11–13, January 2016.

[38] N. L. Piparo and M. Razavi, "Long-distance trust-free quantum key distribution," *IEEE Journal of Selected Topics in Quantum Electronics*, vol. 21, pp. 123–130, May 2015.

[39] A. Delteil, Z. Sun, W.-b. Gao, E. Togan, S. Faelt, and A. Imamoglu, "Generation of heralded entanglement between distant hole spins," *NATURE PHYSICS*, vol. 12, pp. 218+, MAR 2016.

[40] B. T. Kirby, S. Santra, V. S. Malinovsky, and M. Brodsky, "Entanglement swapping of two arbitrarily degraded entangled states," *PHYSICAL REVIEW A*, vol. 94, JUL 20 2016.

[41] T. Shang, J. Li, Z. Pei, and J.-w. Liu, "Quantum network coding for general repeater networks," *Quantum Information Processing*, vol. 14, no. 9, pp. 3533–3552, 2015.

[42] H. V. Nguyen, S. X. Ng, and L. Hanzo, "Irregular convolution and unity-rate coded network-coding for cooperative multi-user communications," *IEEE Transactions on Wireless Communications*, vol. 12, no. 3, pp. 1231–1243, 2013.

[43] Q. You, Y. Li, and Z. Chen, "Joint relay selection and network coding for error-prone two-way decode-and-forward relay networks," *IEEE Transactions on Communications*, vol. 62, pp. 3420–3433, Oct 2014.

[44] T. X. Vu, P. Duhamel, and M. D. Renzo, "On the diversity of network-coded cooperation with decode-and-forward relay selection," *IEEE Transactions on Wireless Communications*, vol. 14, pp. 4369–4378, Aug 2015.

[45] M. Hayashi, *Quantum Information*. Springer, 2006.

[46] M. M. Wilde, *Quantum Information Theory*. Cambridge University Press, 2013.

[47] M. A. Nielsen and I. L. Chuang, *Quantum Computation and Quantum Information*. Cambridge University Press, 2010.

[48] H. V. Nguyen, Z. Babar, D. Alanis, P. Botsinis, D. Chandra, S. X. Ng, and L. Hanzo, "EXIT-chart aided quantum code design improves the normalised throughput of realistic quantum devices," *IEEE Access*, vol. 4, pp. 10194–10209, 2016.

Hung Viet Nguyen received the B.Eng. degree in Electronics & Telecommunications from Hanoi University of Science and Technology (HUST), Hanoi, Vietnam, in 1999, the M.Eng. in Telecommunications from Asian Institute of Technology (AIT), Bangkok, Thailand, in 2002 and the Ph.D. degree in wireless communications from the University of Southampton, Southampton, U.K., in 2013. Since 1999 he has been a lecturer at the Post & Telecommunications Institute of Technology (PTIT), Vietnam. He is involved in the OPTIMIX and CONCERTO European projects. He is currently a postdoctoral researcher at Southampton Wireless (SW) group, University of Southampton, UK. His research interests include cooperative communications, channel coding, network coding, quantum error correction, quantum key distribution, quantum receiver and quantum network coding.

Zunaira Babar received her B.Eng. degree in electrical engineering from the National University of Science & Technology (NUST), Islamabad, Pakistan, in 2008, and the M.Sc. degree (Distinction) and the Ph.D degree in wireless communications from the University of Southampton, UK, in 2011 and 2015, respectively. Her research interests include quantum error correction codes, channel coding, coded modulation, iterative detection and cooperative communications.

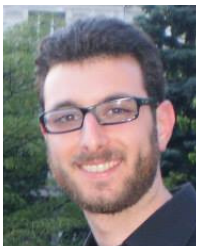

Dimitrios Alanis (S'13) received the M.Eng. degree in Electrical and Computer Engineering from the Aristotle University of Thessaloniki in 2011 and the M.Sc. and PhD degrees in Wireless Communications from the University of Southampton in 2012 and 2017, respectively. He is currently working as a Research Fellow in Southampton Wireless (SW) group, School of Electronics and Computer Science of the University of Southampton, UK. His research interests include quantum computation and quantum information theory, quantum search algorithms, cooperative communications, resource allocation for self-organizing networks, bio-inspired optimization algorithms and classical and quantum game theory.

Panagiotis Botsinis (S'12-M'16) received the M.Eng. degree from the School of Electrical and Computer Engineering of the National Technical University of Athens (NTUA), Greece, in 2010, as well as the M.Sc. degree with distinction and the Ph.D. degree in Wireless Communications from the University of Southampton, UK, in 2011 and 2015, respectively. He is currently working as a Research Fellow in the Southampton Wireless group at the School of Electronics and Computer Science of the University of Southampton, UK. Since October 2010, he has been a member of the Technical Chamber of Greece. His research interests include quantum-assisted communications, quantum computation, iterative detection, OFDM, MIMO, multiple access systems, coded modulation, channel coding, cooperative communications, as well as combinatorial optimization.

Daryus Chandra (S'15) received the M.Eng. degree in electrical engineering from Universitas Gadjah Mada, Indonesia, in 2014. He is currently pursuing the Ph.D. degree with the Southampton Wireless Group, School of Electronics and Computer Science, University of Southampton, UK. He is a recipient of scholarship award from the Indonesia Endowment Fund for Education (Lembaga Pengelola Dana Pendidikan, LPDP). His research interests include classical and quantum error correction codes, quantum information, and quantum communications.

Mohd Azri Mohd Izhar received his M.Eng. degree in electrical engineering (communications) from the University of Sheffield, U.K. in 2008 and Ph.D. degree in electrical engineering from the Universiti Teknologi Malaysia (UTM) in 2014. He is currently a senior lecturer with the UTM Kuala Lumpur campus. Since September 2015, he has been a researcher with the Southampton Wireless Group, School of Electronics and Computer Science, University of Southampton, U.K. His current research interests include channel coding, coding theory, joint source-channel coding, cooperative communications, cognitive radio and quantum error correction codes.

Soon Xin Ng (S'99-M'03-SM'08) received the B.Eng. degree (First class) in electronic engineering and the Ph.D. degree in telecommunications from the University of Southampton, Southampton, U.K., in 1999 and 2002, respectively. From 2003 to 2006, he was a postdoctoral research fellow working on collaborative European research projects known as SCOUT, NEWCOM and PHOENIX. Since August 2006, he has been a member of academic staff in the School of Electronics and Computer Science, University of Southampton. He is involved in the OPTIMIX and CONCERTO European projects as well as the IU-ATC and UC4G projects. He is currently an Associate Professor in telecommunications at the University of Southampton. His research interests include adaptive coded modulation, coded modulation, channel coding, space-time coding, joint source and channel coding, iterative detection, OFDM, MIMO, cooperative communications, distributed coding, quantum error correction codes and joint wireless-and-optical-fibre communications. He has published over 200 papers and co-authored two John Wiley/IEEE Press books in this field. He is a Senior Member of the IEEE, a Chartered Engineer and a Fellow of the Higher Education Academy in the UK.

Lajos Hanzo (M'91-SM'92-F'04) received his degree in electronics in 1976 and his doctorate in 1983. In 2009 he was awarded the honorary doctorate "Doctor Honoris Causa" by the Technical University of Budapest. During his 38-year career in telecommunications he has held various research and academic posts in Hungary, Germany and the UK. Since 1986 he has been with the School of Electronics and Computer Science, University of Southampton, UK, where he holds the chair in telecommunications. He has successfully supervised about 100 PhD students, co-authored 20 John Wiley/IEEE Press books on mobile radio communications totalling in excess of 10 000 pages, published 1400+ research entries at IEEE Xplore, acted both as TPC and General Chair of IEEE conferences, presented keynote lectures and has been awarded a number of distinctions. Currently he is directing a 100-strong academic research team, working on a range of research projects in the field of wireless multimedia communications sponsored by industry, the Engineering and Physical Sciences Research Council (EPSRC) UK, the European Research Councils Advanced Fellow Grant and the Royal Societys Wolfson Research Merit Award. He is an enthusiastic supporter of industrial and academic liaison and he offers a range of industrial courses. Lajos is a Fellow of the Royal Academy of Engineering, of the Institution of Engineering and Technology, and of the European Association for Signal Processing. He is also a Governor of the IEEE VTS. During 2008–2012 he was the Editor-in-Chief of the IEEE Press and a Chaired Professor also at Tsinghua University, Beijing. He has 30 000+ citations. For further information on research in progress and associated publications please refer to http://www.wireless.ecs.soton.ac.uk.

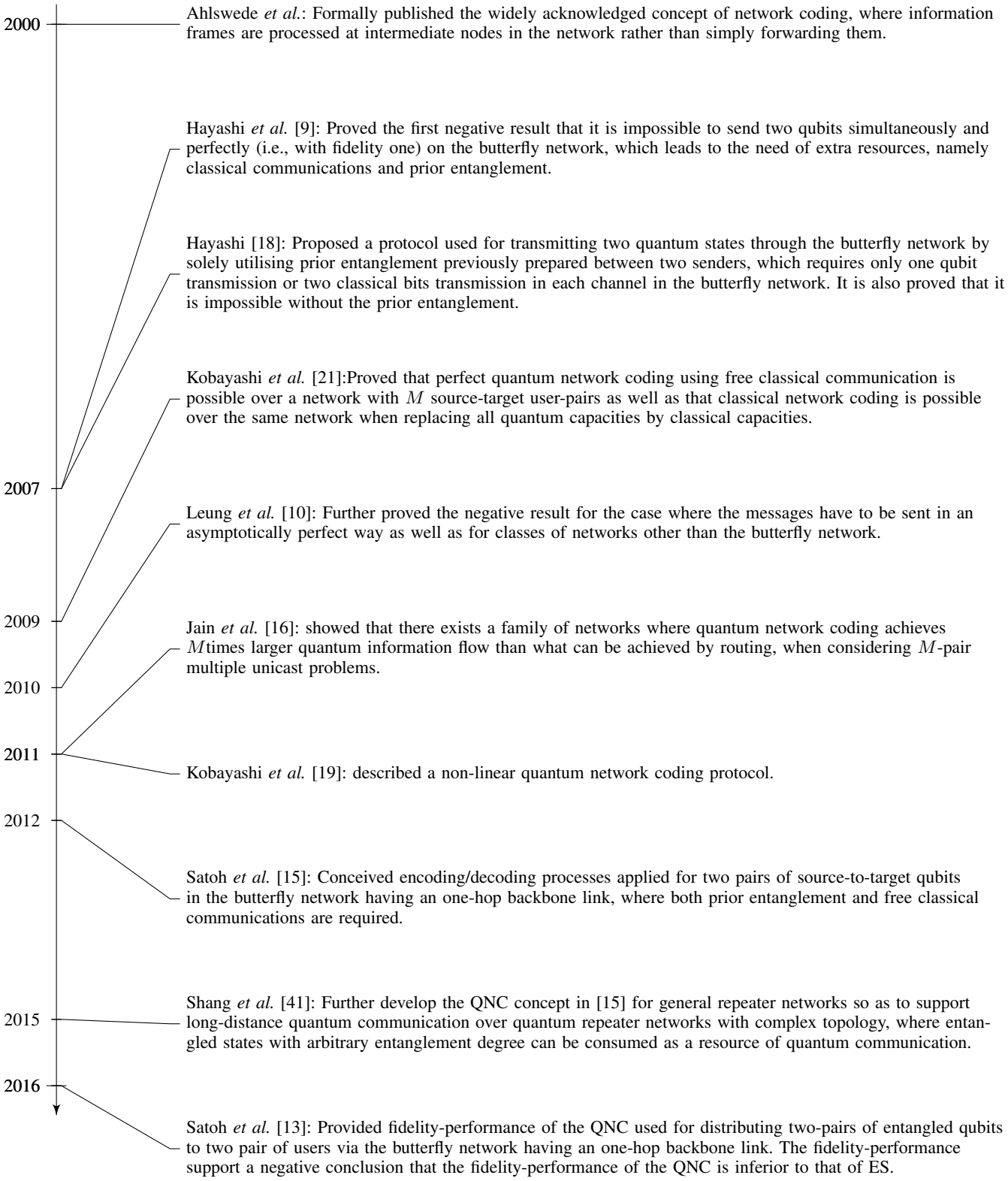

Fig. 1: Milestones of Quantum Network Coding (QNC).

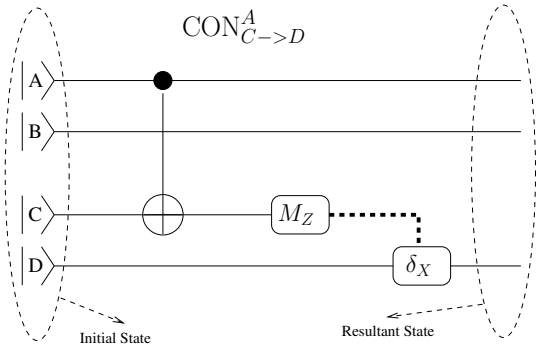

(a) Connection (CON) operation principle, as detailed in Fig. 2(b).

Step	CONnection Manipulation
1	CNOT$_{A->C}$
2	Z-measurement M^Z of $\|C\rangle$ and the use of the result to control δ_X upon $\|D\rangle$

(b) CONnection manipulations illustrated in Fig. 2(a).

Fig. 2: Connection (CON) operation.

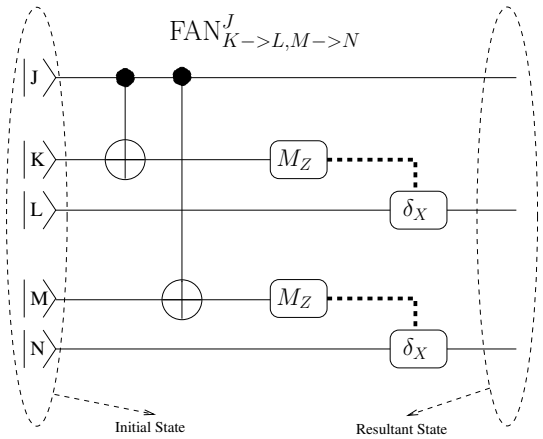

(a) FANout (FAN) operation principle, as detailed in Fig. 4(b).

Step	FANout Manipulation
1	CNOT$^{J->K}$
2	CNOT$^{J->M}$
3	Z-measurement M_Z on $\|K\rangle$ and then use the result to control δ_X upon $\|L\rangle$
4	Z-measurement M_Z on $\|M\rangle$ and then use the result to control δ_X upon $\|N\rangle$

(b) FANout $\mathrm{FAN}^{J}_{K->L,M->N}$ manipulations portrayed in Fig. 4(a).

Fig. 4: Fanout operation.

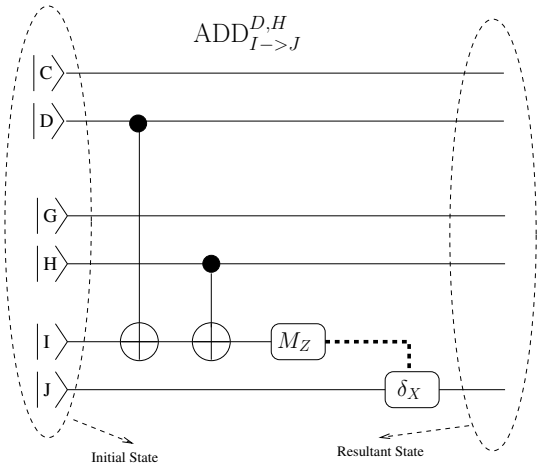

(a) Addition (ADD) operation principle, as detailed in Fig. 3(b).

Step	ADD Manipulations
1	CNOT$_{D->I}$
2	CNOT$_{H->I}$
3	Z-measurement M_Z on $\|I\rangle$ and the use of the result to control δ_X upon $\|J\rangle$

(b) Addition manipulations illustrated in Fig. 3(a).

Fig. 3: Addition operation.

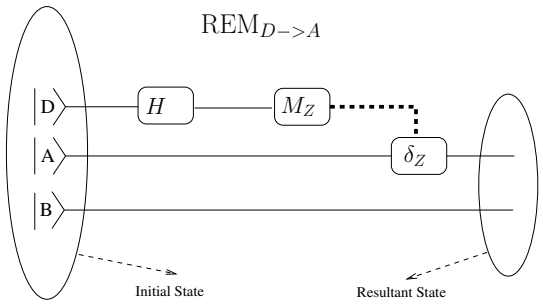

(a) Removal (REM) operation principle, as detailed in Fig. 5(b).

Step	REM Manipulations
1	Hadamard gate is applied to the resource qubit $\|D\rangle$
2	Z-measurement M_Z on $\|D\rangle$ and then use of the result to control δ_Z upon $\|A\rangle$

(b) REMoval REM$_{D->A}$ manipulations illustrated in Fig. 5(a).

Fig. 5: Removal operation.

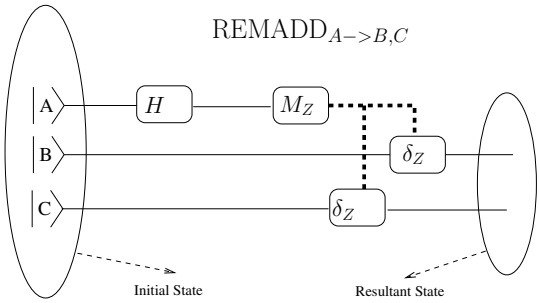

(a) Principle of the remadd (REMADD) operation, as detailed in Fig. 6(b).

Step	REMADD Manipulations
1	Hadamard gate is applied to the resource qubit $\|A\rangle$
2	The resource qubit $\|A\rangle$ then is measured in the Z basis
3	The Z-measurement result is used by δ_Z for controlling $\|B\rangle$ and $\|C\rangle$

(b) REMADD$_{A->B,C}$ manipulations illustrated in Fig. 6(a).

Fig. 6: Removal-and-add operation.

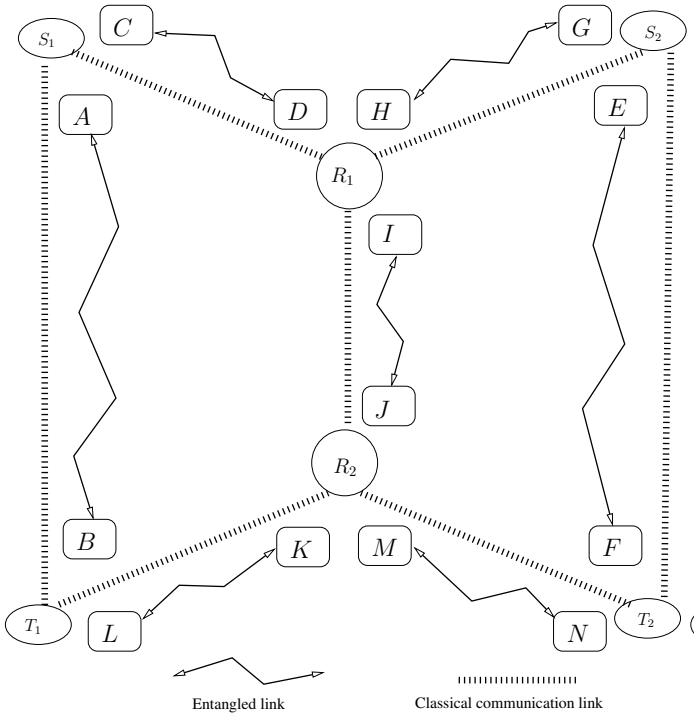

(a) QNC: $N = 1$-hop and $M = 2$-pairs

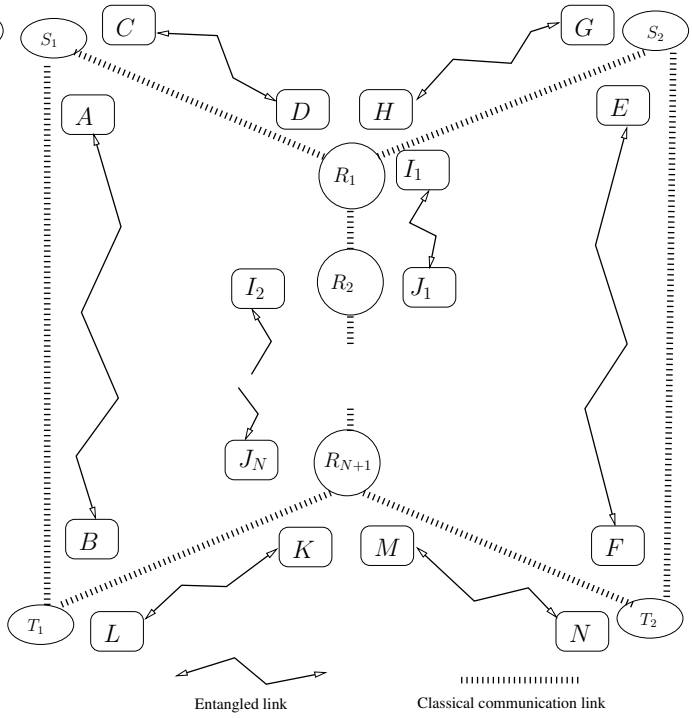

(b) LQNC: $N > 1$-hops and $M = 2$-pairs

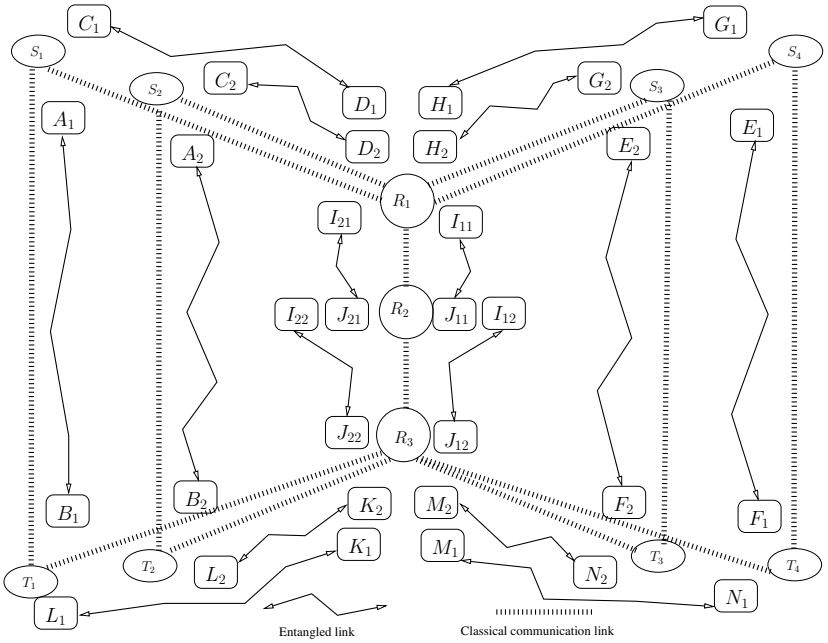

(c) LQNC: $N = 2$-hops and $M = 4$-pairs

Fig. 7: LQNC based schemes having an N-hop backbone link and supporting M pairs of users.

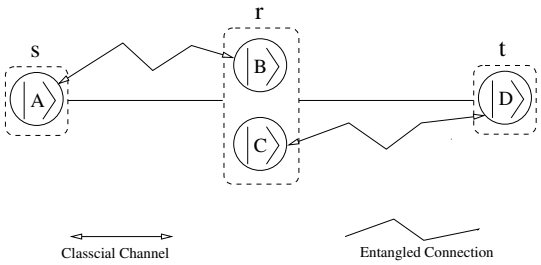

Fig. 8: Schematic of an entanglement swapping based system detailed in Table V

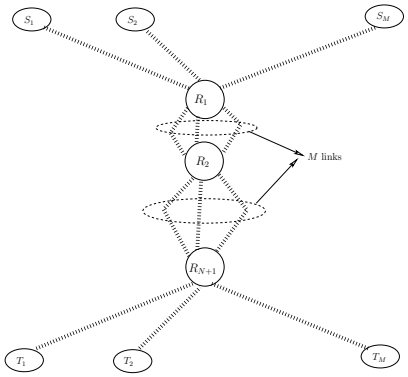

(a) ES: N-hop backbone link and M-pairs

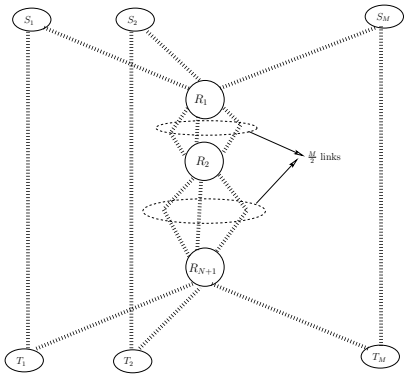

(b) LQNC: N-hop backbone link and M-pairs

Fig. 9: An LQNC-based and an ES-based system, both of which have an N-hop backbone link and support M pairs of users.

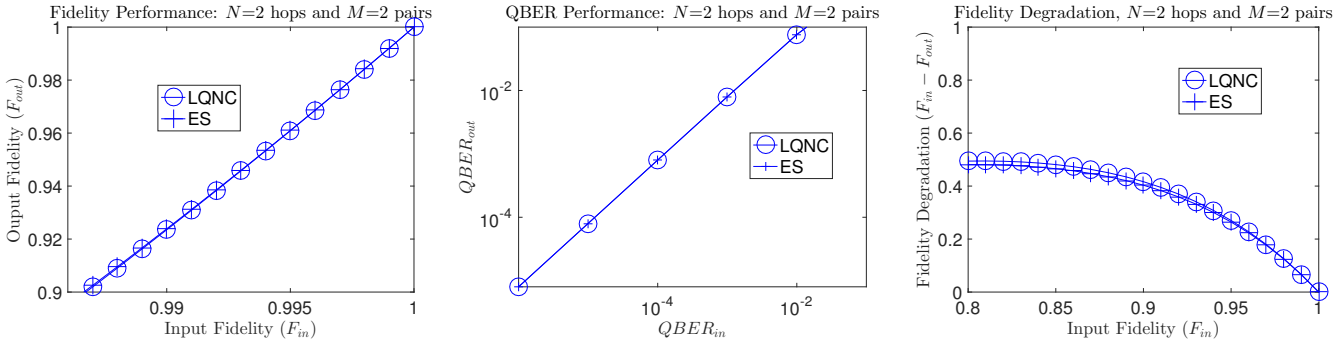

(a) Fidelity: $N = 2, M = 2$ (b) QBER: $N = 2, M = 2$ (c) Fidelity degradation: $N = 2, M = 2$

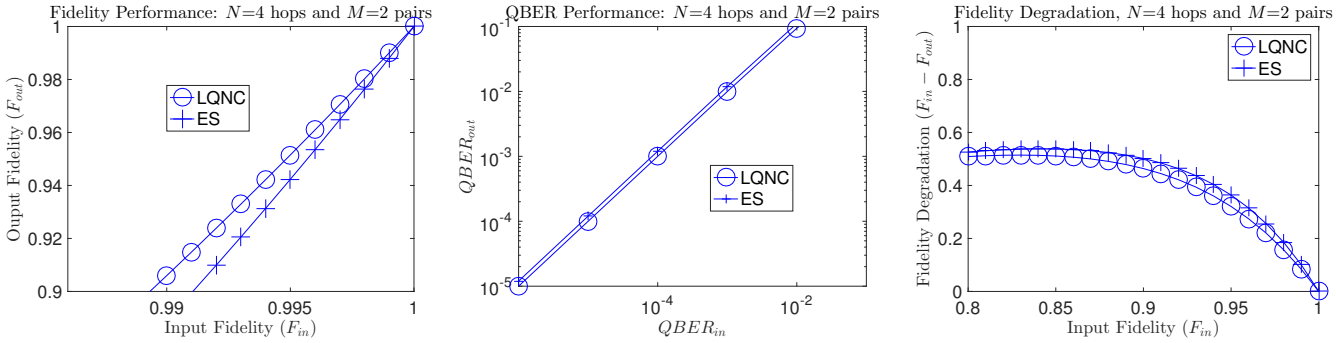

(d) Fidelity: $N = 4, M = 2$ (e) QBER: $N = 4, M = 2$ (f) Fidelity degradation: $N = 4, M = 2$

Fig. 10: Fidelity/QBER/Fidelity-degradation performance of QNC and ES for different numbers of hops ($N = 2, 4$), when considering Z errors in the system supporting $M = 2$ pairs of source-target users.

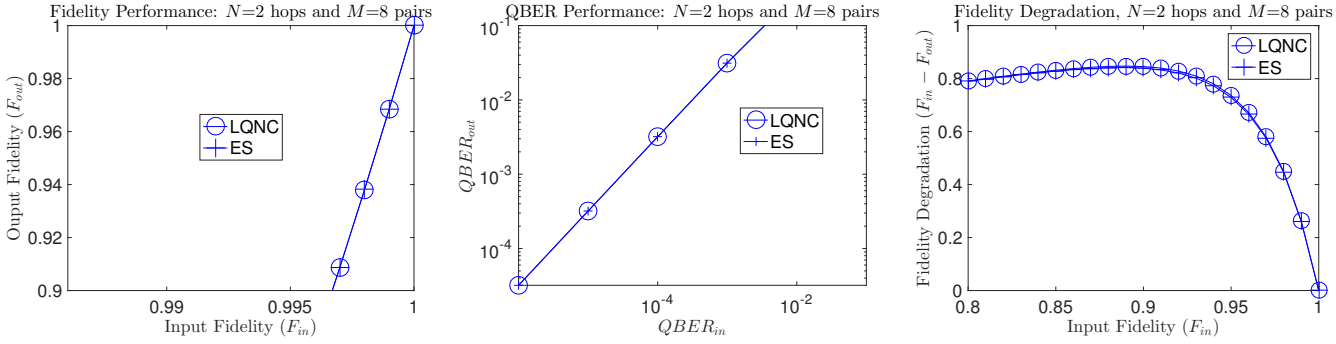

(a) Fidelity: $N = 2, M = 8$ (b) QBER: $N = 2, M = 8$ (c) Fidelity Degradation: $N = 2, M = 8$

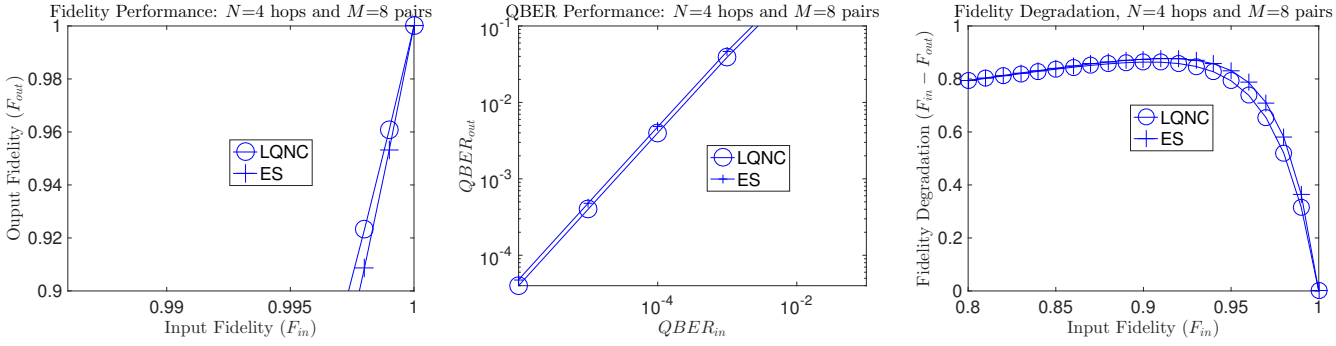

(d) Fidelity: $N = 4, M = 8$ (e) QBER: $N = 4, M = 8$ (f) Fidelity degradation: $N = 4, M = 8$

Fig. 11: Fidelity/QBER/Fidelity-degradation performance of QNC and ES for different numbers of hops ($N = 2, 4$), when considering Z errors in the system supporting $M = 8$ pairs of source-target users.

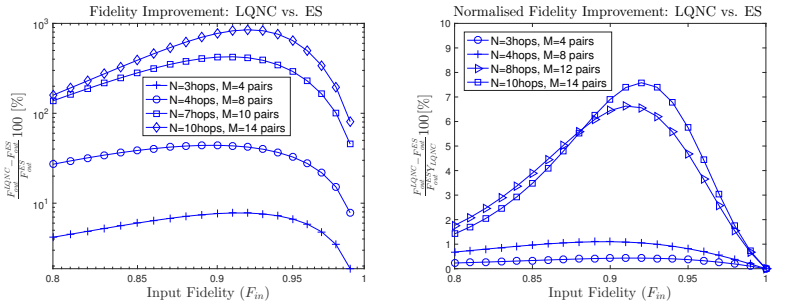

(a) Relative fidelity improvement (b) Normalised relative fidelity improvement

Fig. 12: Fidelity improvement of LQNC-based systems over ES-based systems.